Interim Engineering Report No.4

RESEARCH ON TECHNIQUES FOR LIGHT MODULATION DETECTION

March 1, 1963 to July 1, 1963

D.E. Caddes
B.J. McMurtry
A.E. Siegman
R. Targ

Contract AF 33(657)-8995

The applied research reported in this document has been made possible through support and sponsorship extended by the Electronic Technology Laboratory of the Aeronautical Systems Division, under Contract No. AF 33(657)-8995. It is published for technical information only, and does not necessarily represent recommendations or conclusions of the sponsoring agency.

MICROWAVE DEVICE DIVISION

SYLVANIA ELECTRIC PRODUCTS INC.

MOUNTAIN VIEW, CALIFORNIA

INTERIM ENGINEERING REPORT NO. 4

RESEARCH ON TECHNIQUES FOR LIGHT MODULATION DETECTION

March 1, 1963 to July 1, 1963

BPSN 6799
Contract AF 33(657)-8995

Prepared by

D. E. Caddes
B. J. McMurtry
A. E. Siegman (Consultant)
R. Targ

Approved by

B. J. McMurtry, Head
Optical Device Department

R.G.E. Hutter, Chief Engineer
Microwave Device Division

MICROWAVE DEVICE DIVISION
SYLVANIA ELECTRIC PRODUCTS INC.
500 Evelyn Avenue
Mountain View, California

ABSTRACT

This report covers the fourth quarter of an applied research program conducted by the Sylvania Microwave Device Division to establish techniques for light modulation detection, and it concludes a one year program on amplitude modulation (AM) detectors. The reports on this program provide sufficient information for the detailed understanding, design and use of traveling-wave microwave phototubes (TWP's).

The major topics in this report are: (1) an analysis of the dependence of power output on the large spread in initial velocities from photoelectric cathodes; (2) analysis of the conversion of current modulation to velocity modulation in the gun region of a TWP; (3) detailed calculations of equivalent conductance, G_{eq}, which expresses the way in which velocity modulation is converted to circuit power; (4) comprehensive measurements on TWP's and comparison with detailed theory; (5) suggestion and utilization of a novel technique for measuring R_{eq}; and (6) a summary of research contributions on the AM demodulator program.

TABLE OF CONTENTS

LIST OF ILLUSTRATIONS

LIST OF ILLUSTRATIONS
(CONTINUED)

SECTION I

OBJECTIVE

The objective of this program is to conduct applied research on techniques for light modulation detection. Devices capable of detecting the modulation on a light signal are sought. Consideration will be given to the feasibility of including an amplification process for the detected signal.

SECTION II

TECHNICAL APPROACH AND REPORT OUTLINE

This program requires the investigation of: (1) demodulators for amplitude-modulated (AM) light; (2) demodulators for frequency-modulated (FM) or phase-modulated (PM) light; and (3) optical heterodyne demodulators. Since it seemed unlikely that all three topics could be adequately investigated in a one-year program, it was decided to place major emphasis upon AM demodulators.

In evaluating various approaches the following list of primary desirable characteristics was kept in mind:

(1) Capability of detecting light signals modulated at microwave frequency rates;
(2) Capability of detecting with large modulation bandwidths (greater than 1 Gc);
(3) Suitability for optical heterodyne detection;
(4) Capability of amplification in the light modulation detector;
(5) Low noise detection.

These criteria led to the choice of the traveling-wave phototube (TWP) as the most promising AM demodulator. Investigation of possible slow-wave structures led to the conclusion that the single helix is the most desirable form because of its high interaction impedance and extremely large bandwidth.

The technical program during the past year has consisted of:

(1) Theoretical analysis of TWP's;
(2) TWP construction;
(3) Experimental analysis of TWP's and comparison with theory;
(4) Some theoretical and experimental evaluation of other types of AM demodulators.

This report presents the results of research on AM demodulators for the period from 1 March 1963 to 1 July 1963 and concludes the investigation of AM demodulators.

Since 15 May 1963 the major effort on this contract has been devoted to the investigation of FM demodulators. These investigations will be reported in Interim Engineering Report No.5 dated 1 September 1963.

The remainder of this report is arranged in the following way:

(1) Section III presents recent results of TWP theoretical analysis;

(2) Section IV presents recent results of TWP experimental analysis and compares these results with theory;

(3) Section V presents a summary of research contributions on AM demodulators;

(4) Sections VI - IX present the conclusions, recommendations, plans for the next period, and references, respectively.

SECTION III

THEORETICAL ANALYSIS OF MICROWAVE PHOTOTUBES

3.1 Objective

The objective of this investigation is to examine theoretically the power output, bandwidth, and noise of microwave phototubes.

3.2 Gun Region Analysis

3.2.1 Signal Propagation in the Gun Region

The modulated light input to a microwave phototube produces, of course, an a-c current modulation at the phototube cathode. Before this a-c current modulation can reach the helix, it must pass through the cathode-anode region (or regions) of the electron gun. If the beam current is low, the cathode-anode region is electrically short, and the a-c current is transmitted through the gun region with essentially no change. However, if the beam current is high enough, the gun is electrically long, and the a-c current modulation on the beam will be considerably altered in passing through the gun region. The a-c current will be substantially reduced, and the current modulation partially converted into a-c velocity modulation. Since, for a wide range of TWP parameters, velocity modulation is not as effective in driving the phototube helix as is current modulation, this conversion of current to velocity modulation can adversely affect the phototube performance.

In order to understand quantitatively how the gun region acts to alter the phototube performance, we have performed two analyses of the gun region of a microwave phototube. Before setting down the details of the analyses, let us consider in general terms the gun region itself.

The simplest form for the gun region is a simple planar diode formed by the cathode and the anode of the gun. More complicated guns may have several anodes, which may require that the gun be divided into several successive regions for analysis. We can indicate the general behavior, however, by considering only a simple one-region gun.

Figure 1 shows the potential profile, i.e. the d-c potential versus distance, in such a gun for several different beam currents. As is well known, for very low currents the potential profile is a straight line of slope V_{0A}/d, where V_{0A} is the anode voltage and d the diode spacing. As the d-c current is increased, the potential is increasingly depressed by the space charge associated with the current. Finally, there is a maximum, or space-charge-limited, current, at which the slope of the potential profile becomes zero just in front of the cathode. At this current value, a potential minimum forms in front of the cathode; the diode becomes space-charge-limited; and the current does not increase further. This maximum current occurs at a maximum current density J_{0M} given by Child's Law,

$$J_{0M} = \frac{4\sqrt{2\eta}\,\epsilon\, V_{0A}^{3/2}}{9d^2}$$

Now, when the current is small and the potential profile essentially linear, it can be shown from our analyses that the gun region is electrically short, and the current modulation is transmitted unchanged through the gun region. However, as the current desntiy J_0 approaches J_{0M}, the potential profile approaches the space-charge-limited form; the gun region becomes of appreciable electrical length; and there is

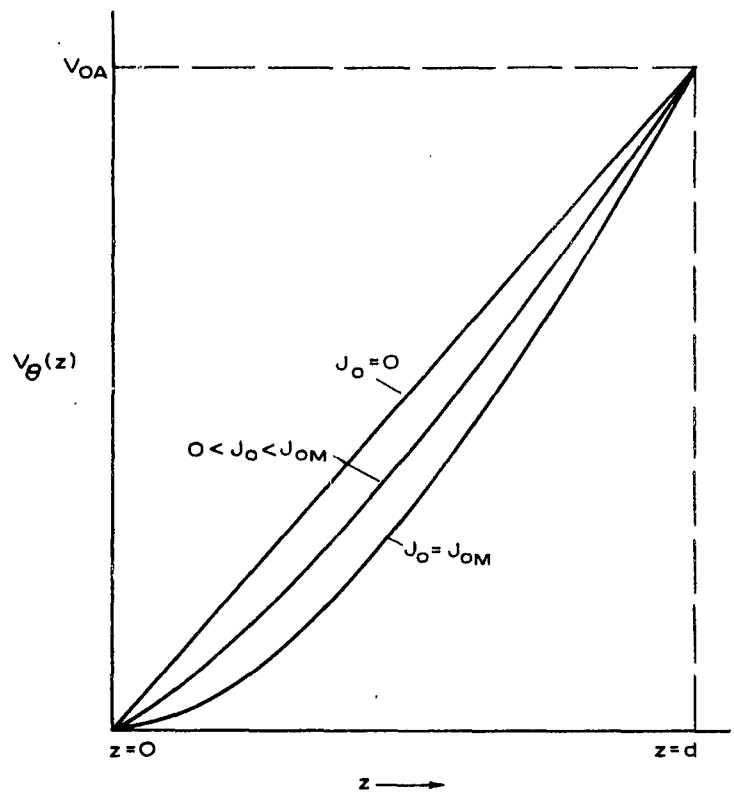

Figure 1. Potential Profiles in a Planar Diode at Different Beam Current Densities.

large conversion of current modulation into velocity modulation in the gun region. In a phototube at high light levels, the photocurrent density J_0 may approach J_{OM}, so this situation is of practical importance.

Note also that the slope of the potential profile at the cathode plane depends on the ratio of the current density J_0 to the maximum current density J_{OM}. The initial slope goes from V_{OA}/d at $J_0 = 0$, to zero at $J_0 = J_{OM}$.

3.2.2 Gun Region Analyses

We have developed two different analyses for the gun region of a microwave phototube, namely:

(1) Smullin[1] gives analytic solutions for the propagation of a-c signals through a one-dimensional planar diode for any degree of space charge. We have adapted his treatment to give analytic expressions for a-c current transmission through a one-region microwave phototube gun. This analysis is relatively simple, but is valid only under the approximations of a one-dimensional, one-region planar diode gun. (Real phototube electron guns are probably reasonably well approximated by this model).

(2) In order to treat more general multi-region electron guns with more complex potential profiles, and in order to take into account finite beam diameters and plasma reduction factors, one must go to the more complicated transmission-line model for signal propagation on an electron beam. For possible future use, we have set down the basic equations of this analysis, and pointed out how they could be applied to the phototube gun region.

3.2.3 One-Dimensional One-Region Planar Diode Analysis

The following analysis is adapted from the paper by Smullin. The

first problem is to find a relationship between the d-c current in the diode and the initial slope of the potential profile at the cathode plane, since this latter parameter is important in later results. We define the initial slope E_0 by

$$E_0 \equiv \left.\frac{dV_0(z)}{dz}\right|_{z=0}$$

(The actual E field at the cathode plane is $-E_0$). Then, Smullin's paper gives the relationship

$$\left(d - \frac{\epsilon^2 \eta E_0^3}{3 J_0^2}\right)^2 =$$

$$\frac{2\epsilon}{9\eta J_0}\left(\sqrt{2\eta V_{0A}} - \frac{\epsilon \eta E_0^2}{J_0}\right)^2 \left(\sqrt{2\eta V_{0A}} + \frac{\epsilon \eta E_0^2}{2 J_0}\right)$$

This expression relates diode current density J_0, diode voltage V_{0A}, diode spacing d, and initial slope E_0. We find that, by proper substitutions, this can be put into the more useful form

$$\left[1 - \frac{27}{32}\left(\frac{E_0 d}{V_{0A}}\right)^3 \left(\frac{J_{0M}}{J_0}\right)^2\right]^2 =$$

$$\left(\frac{J_{0M}}{J_0}\right)\left[1 - \frac{9}{8}\left(\frac{E_0 d}{V_{0A}}\right)^2 \left(\frac{J_{0M}}{J_0}\right)\right]^2 \left[1 + \frac{9}{16}\left(\frac{E_0 d}{V_{0A}}\right)^2 \left(\frac{J_{0M}}{J_0}\right)\right]$$

This now relates the normalized initial slope, $E_0 d/V_{0A}$, to the normalized current density, J_0/J_{0M}. This expression can be solved analytically for the d-c current density as a function of the initial slope, giving

$$\frac{J_o}{J_{oM}} = \frac{1}{2}\left[1 - \sqrt{1 - \frac{27}{4}\left(\frac{E_o d}{V_{oA}}\right)^2\left(1 - \frac{E_o d}{V_{oA}}\right)}\right]$$

$$\text{for} \quad \frac{2}{3} \leq \frac{E_o d}{V_{oA}} \leq 1 \quad ;$$

and

$$\frac{J_o}{J_{oM}} = \frac{1}{2}\left[1 + \sqrt{1 - \frac{27}{4}\left(\frac{E_o d}{V_{oA}}\right)^2\left(1 - \frac{E_o d}{V_{oA}}\right)}\right]$$

$$\text{for} \quad 0 \leq \frac{E_o d}{V_{oA}} \leq \frac{2}{3}$$

The resulting curve of initial slope versus current density is plotted in Figure 2. As noted in the figure, the expressions

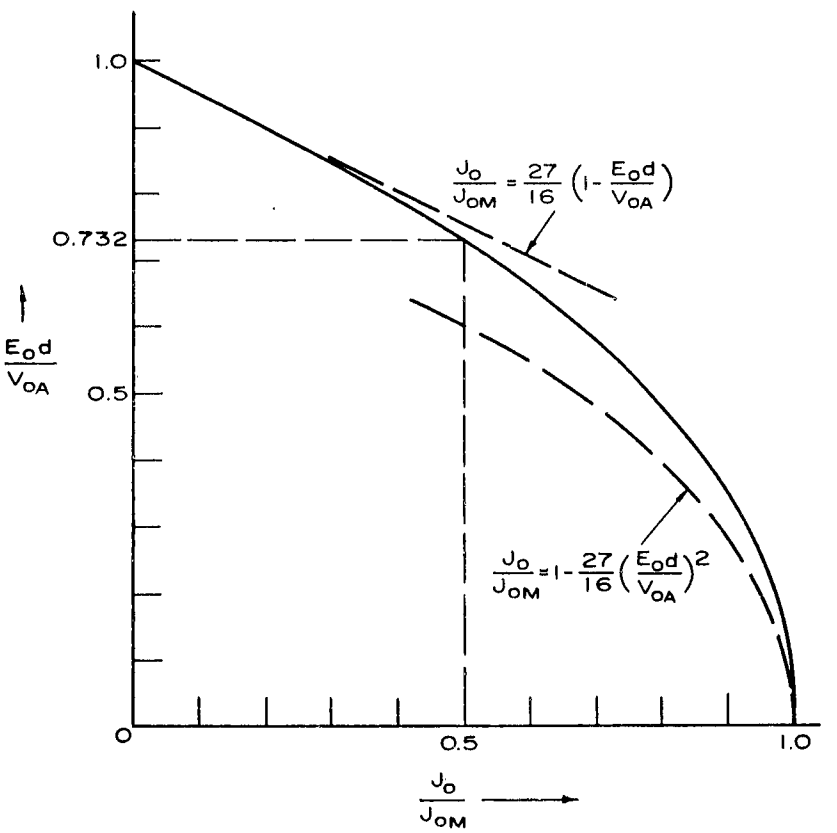

Figure 2. Relationship Between Normalized Current in a Planar Diode and Normalized Slope of the Voltage Profile at the Cathode Plane.

$$\frac{J_o}{J_{om}} \approx \frac{27}{16}\left(1 - \frac{E_{od}}{V_{oA}}\right), \quad \frac{E_{od}}{V_{oA}} \to 1$$

and

$$\frac{J_o}{J_{OM}} \approx 1 - \frac{27}{16}\left(\frac{E_{od}}{V_{oA}}\right)^2, \quad \frac{E_{od}}{V_{oA}} \to 0$$

are limiting cases at the two ends of the curve.

Smullin also gives the following expression for the a-c current i_1 at the anode plane of the gun region, in terms of the a-c current $i_1(0)$ and a-c velocity $v_1(0)$ at the cathode plane:

$$i_1 = \left(\frac{\epsilon\eta E_o^2}{J_o\sqrt{2\eta V_{oA}}}\right)\left[\sqrt{1 + \frac{2J_o\sqrt{2\eta V_{oA}}}{\epsilon\eta E_o^2}} - 1\right] i_1(0)$$

$$+ j\left[\sqrt{1 + \frac{\epsilon\eta E_o^2}{2J_o\sqrt{2\eta V_{oA}}}} - \sqrt{\frac{\epsilon\eta E_o^2}{2J_o\sqrt{2\eta V_{oA}}}}\right]\sqrt{\frac{\epsilon J_o}{2\eta}}\, 2\omega A v_1(0)$$

In this expression, A is the beam cross-sectional area. Smullin gives another, similar expression which relates the a-c velocity v_1 at the anode plane to the velocity and current at the cathode plane. Since we are chiefly interested in the a-c current propagation through the diode, we will not pursue the velocity expression.

Consider the initial current erm in the above equation: after some manipulation, we find that this term can be written

$$\frac{i_1}{i_1(0)} = \frac{9}{8}\left(\frac{E_0 d}{V_{0A}}\right)^2\left(\frac{J_{0M}}{J_0}\right)\left[\sqrt{1+\frac{16}{9}\left(\frac{V_{0A}}{E_0 d}\right)^2\left(\frac{J_0}{J_{0M}}\right)}-1\right]$$

But, since the slope factor $E_0 d/V_{0A}$ is itself a function only of the current parameter J_0/J_{0M}, this result can be written

$$\frac{i_1}{i_1(0)} = \text{function of } \left(\frac{J_0}{J_{0M}}\right) \text{ only}.$$

To find $i_1/i_1(0)$ for any given J_0/J_{0M}, we use Figure 2 to find the slope parameter; then we use both parameters in the above equation for $i_1/i_1(0)$. Figure 3 is a plot of the resulting dependence of the current transmission through the gun region as a function of the amount of d-c current. Note that, as stated earlier, the a-c current transmission is unity for small J_0 and drops to zero as J_0 approaches its maximum value. The expressions

$$\frac{i_1}{i_1(0)} \approx 1 - \frac{4}{9}\frac{J_0}{J_{0M}} \qquad J_0 \ll J_{0M}$$

and

$$\frac{i_1}{i_1(0)} \approx \sqrt{\frac{4}{3}\left(1-\frac{J_0}{J_{0M}}\right)} \qquad J_0 \to J_{0M}$$

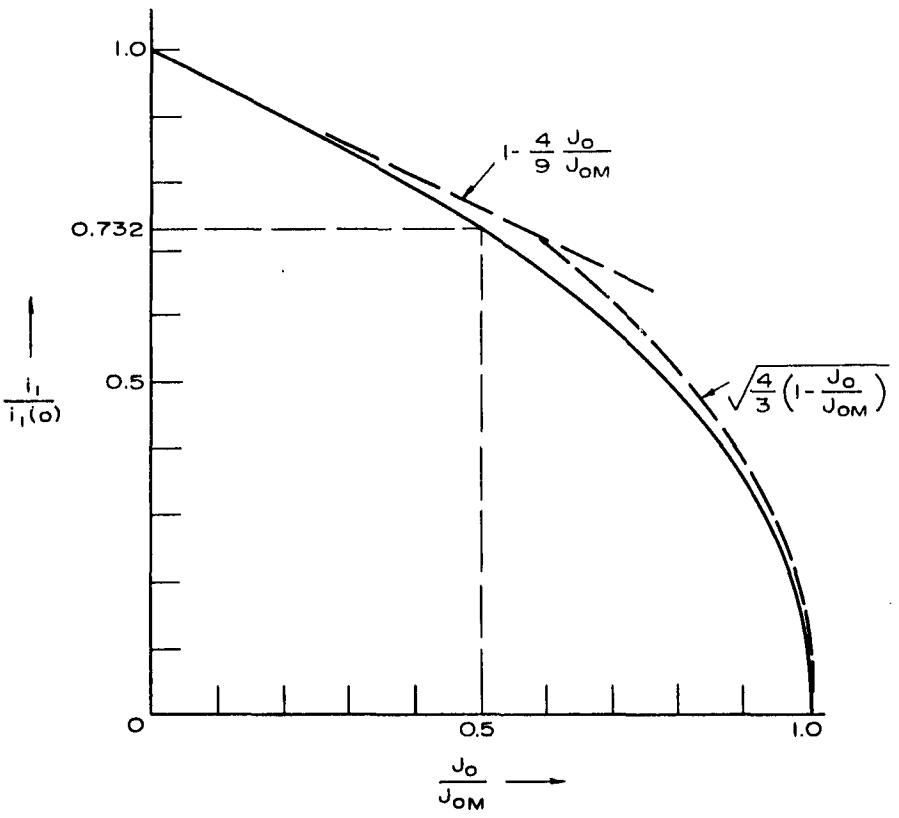

Figure 3. Relationship Between Normalized D-C Current in a Planar Diode and Ratio of A-C Current at Anode Plane to A-C Current at Cathode Plane.

are analytic expressions for the two ends of the range. Also, it can be found that $i_1/i_1(0) = 0.732$ for $J_0 = 1/2J_{OM}$.

According to these results, there will be less than 3 db reduction in the current modulation of a microwave phototube due to gun effects so long as the d-c beam current is less than 1/2 of the space-charge-limited value. We note that as a practical example the SY-4302 microwave phototube has an electron gun which corresponds to a planar diode with diode parameters

Voltage, V_{OA} = 425 volts
Spacing, d = 0.22 inch
Beam diameter = 0.070 inch

Therefore, the maximum or space-charge-limited beam current in this tube (current density times beam area) will be

$$\text{Maximum d-c current} = J_{OM}A = 1.6 \text{ milliamperes}$$

So long as the d-c beam current is less than 800 microamps (a very large TWP current), the current modulation reduction due to the gun region will be small (less than 3 db).

The above analysis can be carried further than we have done here, in order to predict:

(1) the output velocity modulation due to initial current modulation; and the resulting signal output;
(2) the output current and velocity modulation due to initial velocity modulation; and the resulting signal outputs.

These effects are second-order effects which, however, may become important in some situations.

3.2.4 Transmission-Line Analysis of Gun Region Propagation

The more general and powerful way of analysing signal propagation in the gun region is to use the more-or-less exact equations for signal

propagation contained in the transmission-line formulation. This formulation will treat much more general gun regions, but simple analytic answers are correspondingly harder to obtain. We will summarize here the basic equations of this method of analysis, which could later be used (perhaps with computer solutions) to analyse signal propagation in more complicated microwave phototube guns.

Consider the a-c current i_1 and a-c kinetic voltage V_1 on an electron beam. It simplifies the analysis if we immediately remove from these quantities the electronic phase shift or phase dependence, by writing

$$V_1(z) = \tilde{V}(z)\, e^{-j\theta(z)}$$

$$i_1(z) = \tilde{i}(z)\, e^{-j\theta(z)}$$

where

$$\theta(z) = \int_0^z \beta_e(z)\, dz$$

Then, the kinetic voltage and current amplitudes, V and i, are governed by the differential equations

$$\frac{d\tilde{V}}{dz} = j\beta_q^2 \frac{2V_0}{\beta_e I_0}\tilde{i} = j X_b(z)\tilde{i}$$

$$\frac{d\tilde{i}}{dz} = j\frac{\beta_e I_0}{2V_0}\tilde{V} = j B_b(z)\tilde{V}$$

Note that in these equations the quantities β_g, V_0, β_e, X_b and B_b may all be functions of distance z because the beam voltage, beam diameter, and beam surroundings may all be changing with distance. The only requirement is that the variation with distance not be too rapid.

Note for comparison that the usual transmission-line equations for an ordinary transmission line with a-c voltage V and a-c current i are

$$\frac{dV}{dz} = -jXi$$

$$\frac{di}{dz} = -jBV$$

These transmission-line equations are identical to the beam equations except for signs. The equations can be made identical if we equate the beam a-c kinetic voltage $\tilde{V}$ to the transmission-line a-c voltage V, i.e.

$$\tilde{V} = V$$

and if we equate the beam a-c current $\tilde{i}$ to the negative of the transmission-line a-c current, i.e.

$$\tilde{i} = -i$$

A beam with a specified $X_b(z)$ and $B_b(z)$ is then exactly equivalent to a transmission line with $X(z)$ and $B(z)$, if

$$X(z) = X_b(z)$$

$$B(z) = B_b(z)$$

That is, the variation of $\tilde{V}$ and $\tilde{\imath}$ along the beam is the same as the variation of V and $-i$ along the transmission line. Figure 4 illustrates this equivalence. Note that a current of $-i$ in the positive direction on the line is the same as a current of $+i$ in the negative direction.

The ratio of $\tilde{V}/\tilde{\imath}$ at any plane along the beam can be called the a-c impedance of the beam at that point, or

$$\tilde{Z} \equiv \frac{\tilde{V}}{\tilde{\imath}}$$

Note that in the transmission-line analog $\tilde{Z}$ at any point is equivalent to

$$\tilde{Z} = \frac{\tilde{V}}{\tilde{\imath}} = \frac{V}{-i}$$

where V is the voltage on the line at that point and i is the current in the negative direction at the same point. Therefore, $\tilde{Z}$ corresponds exactly to the input impedance which will be seen looking into the line (toward the left) at that point.

For example, the elementary situation in the microwave phototube is that $\tilde{V} = 0$ and $\tilde{\imath} = \tilde{\imath}(0)$ at the cathode plane, and we want $\tilde{V}$ and $\tilde{\imath}$ at some later plane, e.g. the anode plane. This means that the transmission line is short-circuited at the cathode plane, and we want the input impedance at some later plane. Figure 5 shows

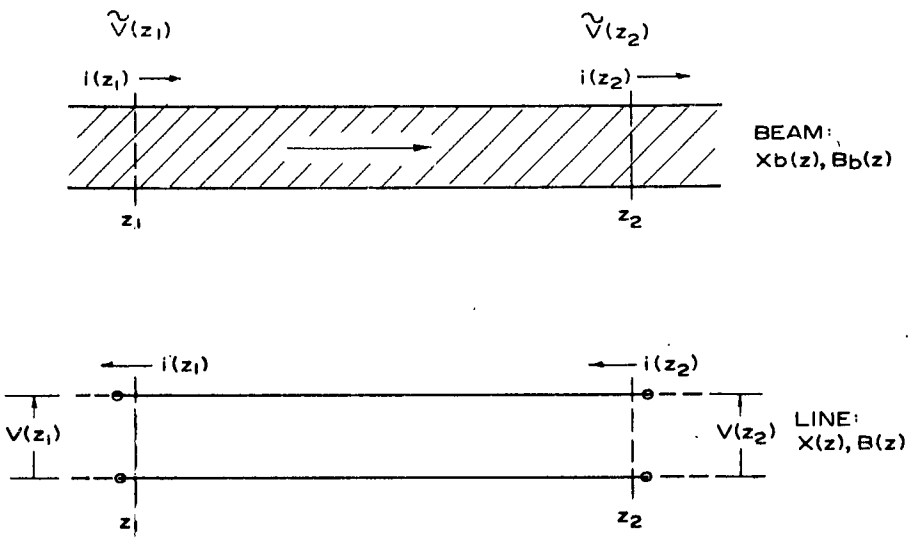

Figure 4. Transmission-Line Analog for and Electron Beam.

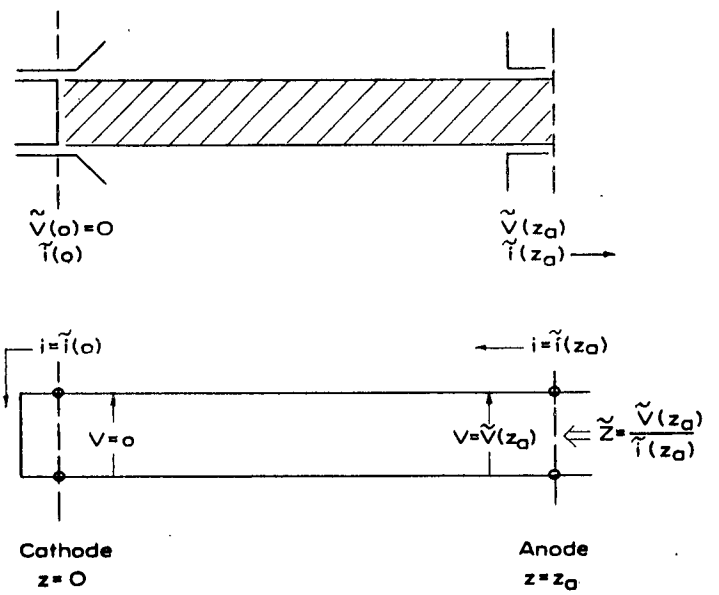

Figure 5. Transmission-Line Analog for a Beam with Pure Current Modulation at the Cathode.

this situation and the corresponding transmission-line analog. The relationship between $\tilde{I}(0)$ and $\tilde{I}(z_a)$ on the beam can be found by calculating (or measuring) the corresponding relationship on the transmission line.

The propagation constant β and the characteristic impedance Z_0 of a transmission line are given by

$$\beta(z) = \sqrt{X(z)\,B(z)}$$

$$Z_0(z) = \sqrt{\frac{X(z)}{B(z)}}$$

or, for the electron beam,

$$\beta_b(z) = \sqrt{X_b(z)\,B_b(z)} = \beta_f(z)$$

$$Z_{0b}(z) = \sqrt{\frac{X_b(z)}{B_b(z)}} = 2\,\frac{\beta_f(z)}{\beta_e(z)}\,\frac{V_0(z)}{I_0}$$

Hence, the beam corresponds directly to a transmission line in which both β and Z_0 vary with distance. It is sometimes easier, particularly in making a real physical analog, if only Z_0 and not β varies with distance. This can be done as follows.

For the electron beam define a "total plasma phase shift" $\phi(z)$

by

$$\phi(z) = \int_0^z \beta_g(z)\, dz$$

Then ϕ can replace z as the measure of distance, or electrical length, along the beam. Similarly, on the transmission line let β be constant with distance, i.e.

$$\beta = \beta_c$$

and define the total phase shift along the line as

$$\phi'(z) = \beta_c z$$

Then, the differential equations for the a-c quantities on the beam become

$$\frac{d\tilde{V}}{d\phi} = j Z_{ob}(\phi)\, \tilde{i}$$

$$\frac{d\tilde{i}}{d\phi} = j Z_{ob}^{-1}(\phi)\tilde{V}$$

$$Z_{ob}(\phi) = 2 \frac{\beta_g(\phi)}{\beta_e(\phi)} \frac{V_o(\phi)}{I_o}$$

where $Z_{ob}(\phi)$, $\beta_q(\phi)$, $\beta_e(\phi)$ and V_o are now considered as functions not of z, but of ϕ. Similarly, the transmission line equations become

$$\frac{dV}{d\phi'} = -j Z_o(\phi') i$$

$$\frac{di}{d\phi'} = -j Z_o^{-1}(\phi') V$$

The beam and the line are now equivalent at the same electrical lengths, i.e. at the points where

$$\phi\Big|_{\text{on the beam}} = \phi'\Big|_{\text{on the line}}$$

provided that they have the same variation of characteristic impedance with electrical length, i.e.

$$Z_{ob}(\phi)\Big|_{\text{on the beam}} = Z_o(\phi')\Big|_{\text{on the line}}$$

Thus, in general, real distance along the line no longer corresponds linearly to real distance along the beam.

There are thus at least two (actually there are many more) ways to represent an electron beam by a transmission line. The first method above seems easier to understand, but the second is somewhat simpler mathematically.

Note that the above equations contain the reduced plasma wavenumber β_q, where

$$\beta_q = p\beta_p \qquad 0 \le p \le 1$$

with $p = p(\beta_e a, \beta_e b)$ being the well-known plasma reduction factor. This factor is one of the reasons why this transmission-line approach is more general, and also more complicated.

In this section, we have set up the transmission-line analysis and indicated how it can be used. Actual solutions have not as yet been carried out. Whether these are necessary or desirable should be the subject of future study.

3.3 Effects of Velocity Spread

We will consider the effects of velocity spread in the electron beam on the microwave phototube equivalent resistance for two regimes of operation: the low-current or constant-R_{eq} regime, and the high-current or growing-wave regime.

3.3.1 Low-Current Regime of Operation

The low-current regime can be treated analytically as follows. The coupled-mode equation for the circuit wave amplitude Φ is

$$\left(\frac{d}{dz} + j\beta_c\right)\Phi = -C_{12}(\rho - 6)$$

where β_c is the circuit propagation constant. In the low-current regime, ρ and 6 have essentially constant amplitude through the tube, but vary in phase with distance as

$$(\rho - 6) = (\rho - 6)_0\, e^{-j\beta_e z}$$

Therefore,

$$\left(\frac{d}{dz} + j\beta_c\right)\Phi = -C_{12}(\rho - 6)_0\, e^{-j\beta_e z}$$

The solution to this equation is

$$\Phi(z) = -C_{12}(\rho - 6)_0 L\, e^{-j\beta_c z} \frac{1}{L} \int_0^z e^{j(\beta_c - \beta_e)z}\, dz$$

of, at the output ($z = L$)

$$\Phi(L) = -C_{12}(\rho - 6)_0 L\, e^{-j\beta_c L} \frac{e^{j\Delta\beta L} - 1}{j\Delta\beta L}$$

$$= -C_{12}(\rho - 6)_0 L\, e^{-j(\beta_c + \beta_e)L/2}\, \mathrm{sinc}(\Delta\beta L/2)$$

where

$$\Delta\beta \equiv \beta_c - \beta_e \quad ; \quad \text{sinc } x \equiv x^{-1} \sin x$$

It is apparent that asynchronism causes a reduction in the output wave amplitude given by

$$R(\Delta\beta L) = \frac{e^{j\Delta\beta L} - 1}{j\Delta\beta L} = \text{REDUCTION IN } \Phi$$

Since output power is proportional to $|\Phi|^2$, the power reduction due to asynchronism between beam and circuit waves is thus

$$\text{Asynchronism power reduction factor, } |R|^2 = \text{sinc}^2(\Delta\beta L/2)$$

Now, if the beam has a velocity spread, some portions of the beam current are necessarily out of synchronism. Suppose the beam current has a velocity distribution, that is a distribution of β_e values of width $\Delta\beta_e$ about an average value β_{eo}, as shown in Figure 6. (This particular distribution is easy to analyse and will indicate the general magnitude of velocity-spread effects.) We assume the a-c modulation is uniform across the distribution. Each incremental range of current in the distribution will have a different amplitude reduction given by

$$R(\Delta\beta L) = \frac{e^{j(\beta_c - \beta_e)L} - 1}{j(\beta_c - \beta_e)L} = \text{amplitude reduction for current element with velocity u}$$

What we need is this reduction factor averaged over all values of where there is current; and then squared, to give power reduction. That is,

$$\overline{|R|^2} = \left|\begin{matrix}\text{AVERAGE}\\ \text{AMPLITUDE}\\ \text{REDUCTION}\end{matrix}\right|^2 = \left| \frac{1}{\Delta\beta_e} \int_{\beta_{eo} - \Delta\beta_e/2}^{\beta_{eo} + \Delta\beta_e/2} R(\Delta\beta L)\, d\beta_e \right|^2$$

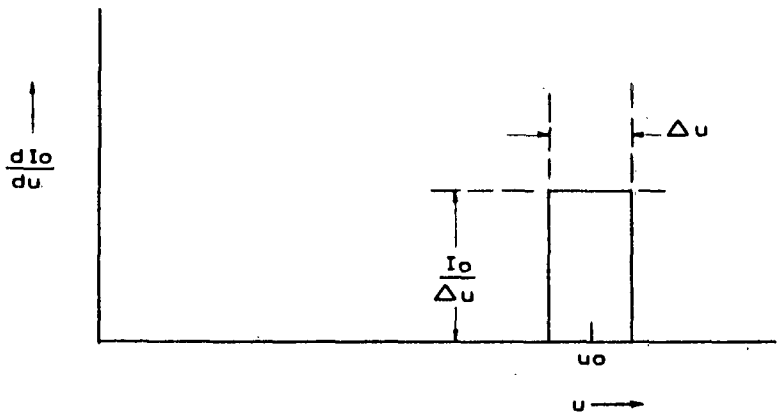

Figure 6. Square Electron-Velocity Distribution.

To simplify this, we assume that the circuit wave is synchronous with the average election velocity, i.e.

$$\beta_c = \beta_{eo} = \omega / u_o$$

and then write

$$y = (\beta_c - \beta_e) L$$

$$dy = - L \, d\beta_e$$

The equation reduces to

$$\overline{|R|^2} = \left| \frac{1}{\Delta\beta L} \int_{-\Delta\beta L/2}^{\Delta\beta L/2} \frac{e^{jy} - 1}{jy} \, dy \right|^2$$

$$\simeq \left| 1 - \frac{1}{2} (\Delta\beta L/6)^2 \right|^2 , \quad \frac{\Delta\beta L}{2} << 1$$

$$\simeq 1 - (\Delta\beta L/6)^2$$

It will be easier to interpret this if we relate the spread in β to the spread ΔV_o in the beam voltage V_o. The relationship (for small fractional widths) is

$$\Delta\beta L \simeq \frac{\beta_e L}{2} \frac{\Delta V_o}{V_o} = (\pi N) \frac{\Delta V_o}{V_o}$$

Hence, the reduction is

$$\overline{|R|^2} \simeq 1 - \left(\frac{N}{2} \frac{\Delta V_o}{V_o} \right)^2$$

The main conclusion of this analysis is that velocity spread effects in usual phototubes should be negligible, because the term which subtracts from unity in the preceding expression is negligible. A reasonable set of parameters might be, for example:

$N = 20$

ΔV_o = 1 volt (typical initial velocity spread of photoelectrons)

V_o = 400 volts

and hence a decrease in signal power by a fractional amount

$$\left(\frac{N}{2}\ \frac{\Delta V_o}{V_o}\right)^2 = \left(\frac{1}{40}\right)^2 = \frac{1}{1600}$$

The only time velocity spread effects will be important will be for very long tubes (large N) having very low helix voltages.

3.3.2 High-Current Regime of Operation

In the high-current regime of operation, the microwave phototube is operating essentially like an ordinary traveling-wave tube, except for slightly different initial conditions. Now, it has been established in traveling-wave tube theory that beam velocity spread acts essentially like a small amount of additional space charge (additional QC). Moreover, the effect of this on TWT gain is essentially negligible.

Hence, we conclude that the effects of velocity spread on the microwave phototube at high currents can equally well be considered as a small increase in QC, with a negligible effect on the output.

3.4 Detailed Calculation of Equivalent Conductance

In Interim Engineering Report No. 3, two of the three possible "pure" excitations of the system consisting of a longitudinal electron beam and a slow wave circuit were discussed in some detail; these were pure circuit power input, corresponding to the traveling-wave amplifier (TWT), and pure current modulation of the beam, representing the traveling-wave phototube (TWP) at low average current. Velocity modulation of the beam, the third "pure" excitation, was introduced, but no data for this case were available at that time. We shall now present these data and draw some conclusions about the importance of velocity modulation in TWP's. Symbols are defined in the glossary and were discussed in detail in previous reports.

Recall that the efficiency of the beam circuit system in producing circuit power output from a velocity modulation input can be described by a transfer function, the "equivalent conductance" (G_{eq}), which takes into account the circuit length and loss, space-charge effects, beam velocity, and beam-circuit coupling coefficient:

$$P_{OUT} = \frac{1}{2} |V_1(0)|^2 \, G_{eq}$$

where $V_1(0)$ is the kinetic beam voltage at $z = 0$, the system input. It is related to the peak velocity modulation on the beam by

$$V_1 = \frac{u_o}{\eta} v$$

Interim Engineering Report No. 3 showed how the high-speed digital

computer solutions for the general beam-circuit problem could readily be used to compute the product of the equivalent conductance and the beam-circuit interaction impedance, $G_{eq}Z_c$. This calculation has been made for the same ranges of tube parameters as the corresponding current modulation quantity, the ratio of the equivalent resistance to the interaction impedance (R_{eq}/z_c), allowing us to directly compare the two types of excitation for various circuit lengths and losses, space-charge conditions, beam velocities, and beam-circuit coupling coefficients.

Another interesting comparison of the G_{eq} computer data is with the simpler theory given in Interim Engineering Report No. 2. Under the restrictions of small C, no loss, synchronous velocity and negligible space charge effects, we found

$$\frac{R_{eq}}{Z_c} = \frac{1}{36C^2} F_+$$

$$G_{eq} Z_c = \frac{C^2}{9} F_-$$

where

$$F_\pm = 1 + 3\sinh^2(\sqrt{3}\pi CN) + \cosh^2(\sqrt{3}\pi CN)$$
$$\pm 2\sqrt{3}\left[4\cos^2(\pi CN) - 1\right]\sinh(\sqrt{3}\pi CN)\sin(\pi CN)$$
$$+ 2\left[4\sin^2(\pi CN) - 1\right]\cosh(\sqrt{3}\pi CN)\cos(\pi CN)$$

For CN $\leq$ 0.3, these reduce to

$$R_{eq}/Z_c \simeq \pi^2 N^2$$

$$G_{eq} Z_c \simeq 4\pi^4 N^4 C^6$$

$$\frac{P_{OUT}(\text{cur. mod.})}{P_{OUT}(\text{vel. mod})} \simeq (4\pi^2 N^2 Q C^3)^{-1}$$

We shall refer to these formulae again in this report, to show their agreement with the more accurate theory programmed for the digital computer.

Figures 7 and 8 show the dependence of G_{eq} on beam velocity. The most obvious effect is the "peaking" which occurs as the length is increased. The same kind of effect was observed in the R_{eq} curves, but comparison with Figures 1 and 2 of Interim Engineering Report No. 3 reveals a significantly stronger effect in the current modulation case. This indicates weaker beam-circuit interaction with a velocity-modulation input, which agrees with the excitation "hierarchy" we established from the simpler theory of Interim Engineering Report No. 2: the current modulation input is better than the velocity modulation input, which is in turn superior to the circuit power input. The other important features of these curves are the increase in power output and the greater influence of Q for longer circuits; the greater lengths allow more energy to be taken from the beam by the circuit and at the same time demand more energy storage in "passive" circuit modes.

A qualitative comparison of Figure 9 , which shows the influence of the gain parameter C, with Figure 3 of Interim Engineering Report No. 3

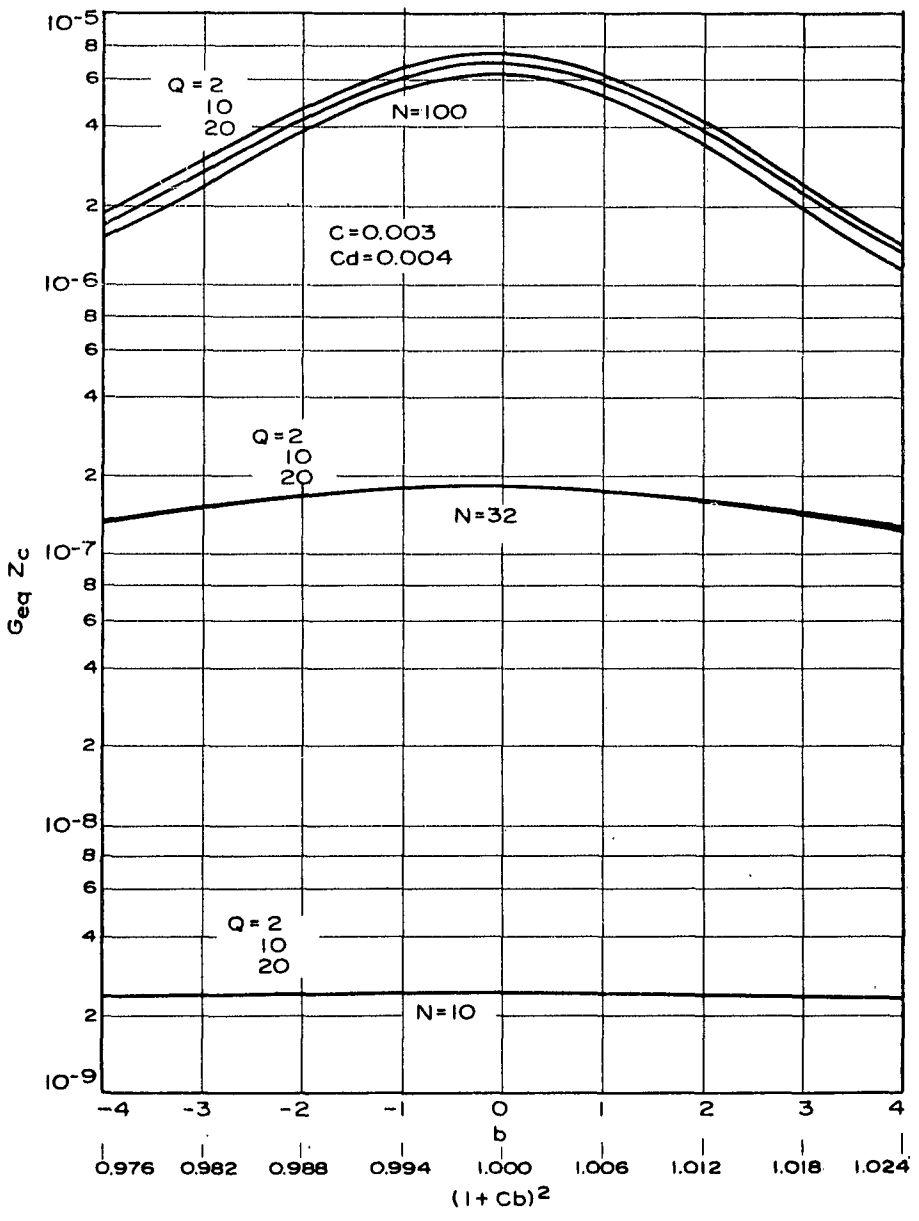

Figure 7. Effect of Beam Velocity Variations on Equivalent Conductance.
c = 0.003, Cd = 0.004

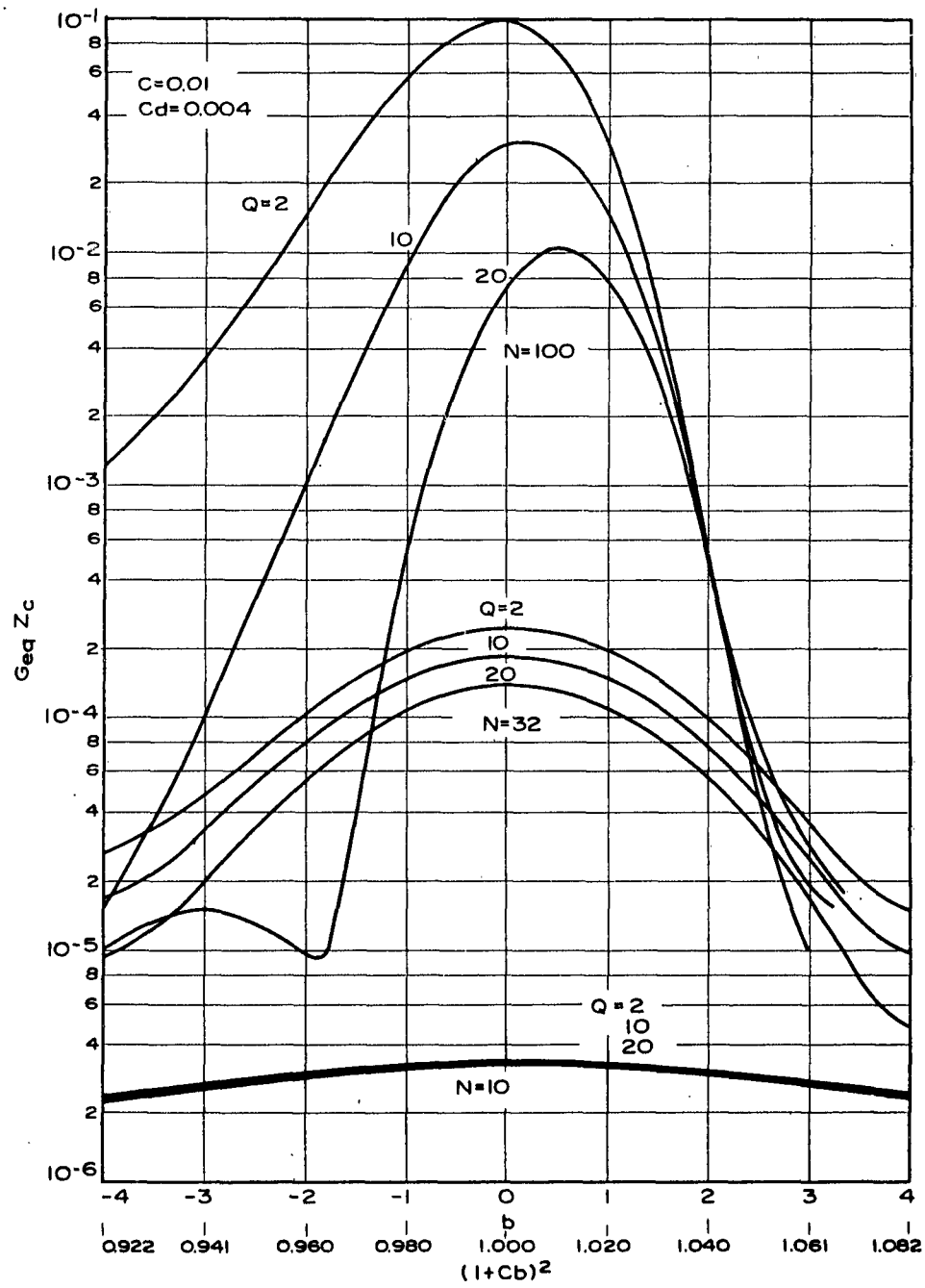

Figure 8. Effect of Beam Velocity Variations on Equivalent Conductance
C = 0.010, Cd = 0.004

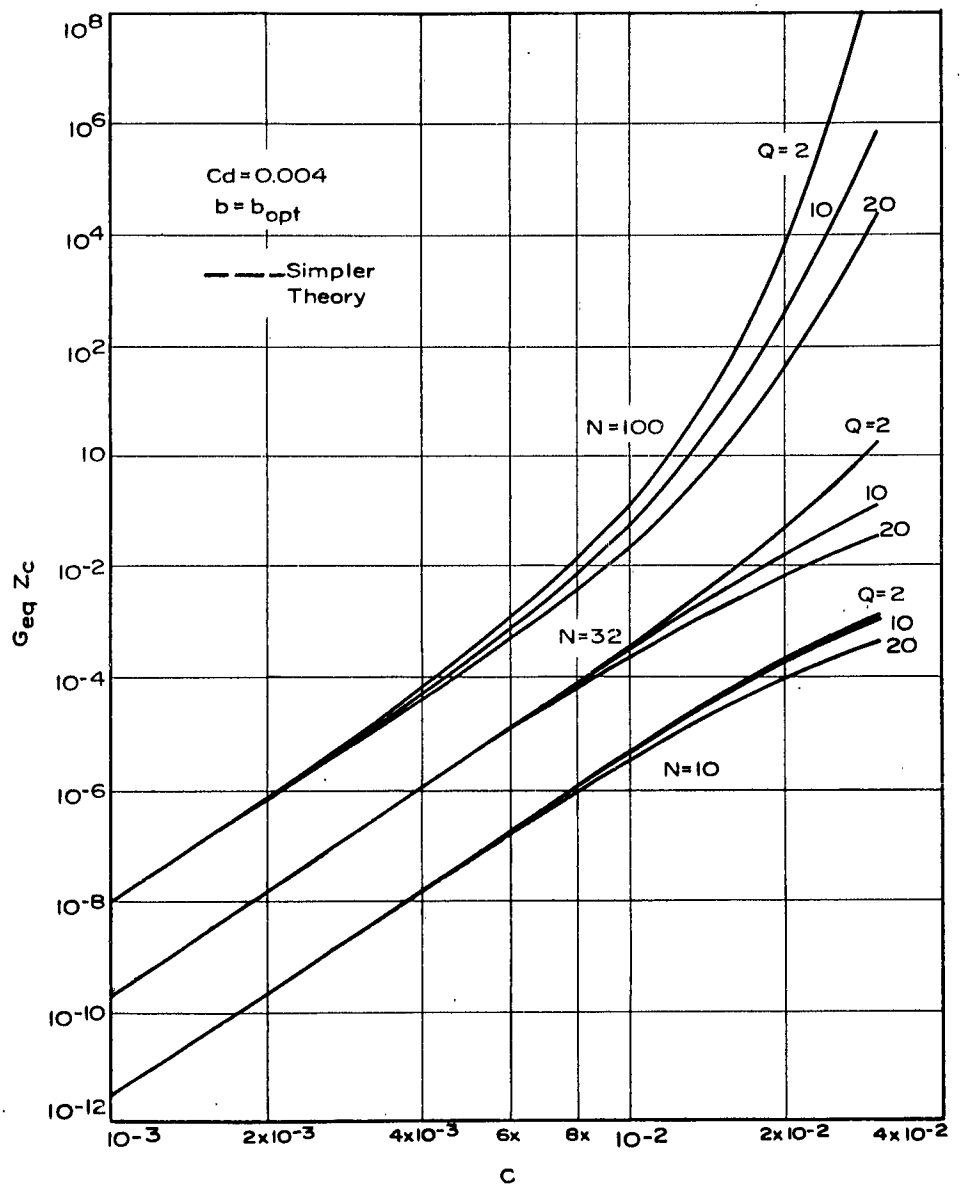

Figure 9. Dependence of Equivalent Conductance Upon the Pierce Gain Parameter, C. Cd = 0.004, b = optimum value for each C, N, Q.

shows an important difference between the two types of excitation. For low C, as predicted by the simpler theory, G_{eq} varies as C^6 while R_{eq} is independent of C; this means that the advantage of current modulation excitation is most marked at low beam current (low C) levels. It also shows that G_{eq} is "catching up" as C increases and poses the question of how closely the current modulation efficiency is approached. In Figure 10 we have plotted the ratio of the circuit power outputs resulting from equivalent amounts of the respective excitations. At small CN we see good agreement with the simpler theory: the ratio varies as C^3N^2 in this region. As exponential growth begins (near $CN \simeq 0.3$) the ratio tends to unity and the two types of input are essentially equivalent as regards their generation of circuit power output. The dotted portions of the graphs are relatively uncertain because we have few data points in this region, but it is not surprising that the space-charge effects which are prominent in both R_{eq} and G_{eq} influence Pcm/Pvm. These curves show that, for the small C and moderate N typical of percent of TWPs, current modulation is clearly the superior type of excitation. They also show that the conversion of current modulation to velocity modulation which occurs in short distances for higher currents is not such a serious detriment as one might expect. At these current levels the velocity modulation input is essentially as good as current modulation.

The influence of circuit length, N, on G_{eq} is shown in Figure 11. For the shorter lengths we observe the N^4 dependence predicted by the simpler theory. The most striking contrast between these curves and Figure 4 of Interim Engineering Report No. 3 is that R_{eq} reaches the exponential growth region at smaller N than does G_{eq}. This is, of course, due to the more efficient transfer of energy from beam to circuit in the current modulation case.

Figure 12 shows how circuit loss lowers G_{eq}; longer circuits are more severely affected by loss. The reason the G_{eq} reduction is more moderate

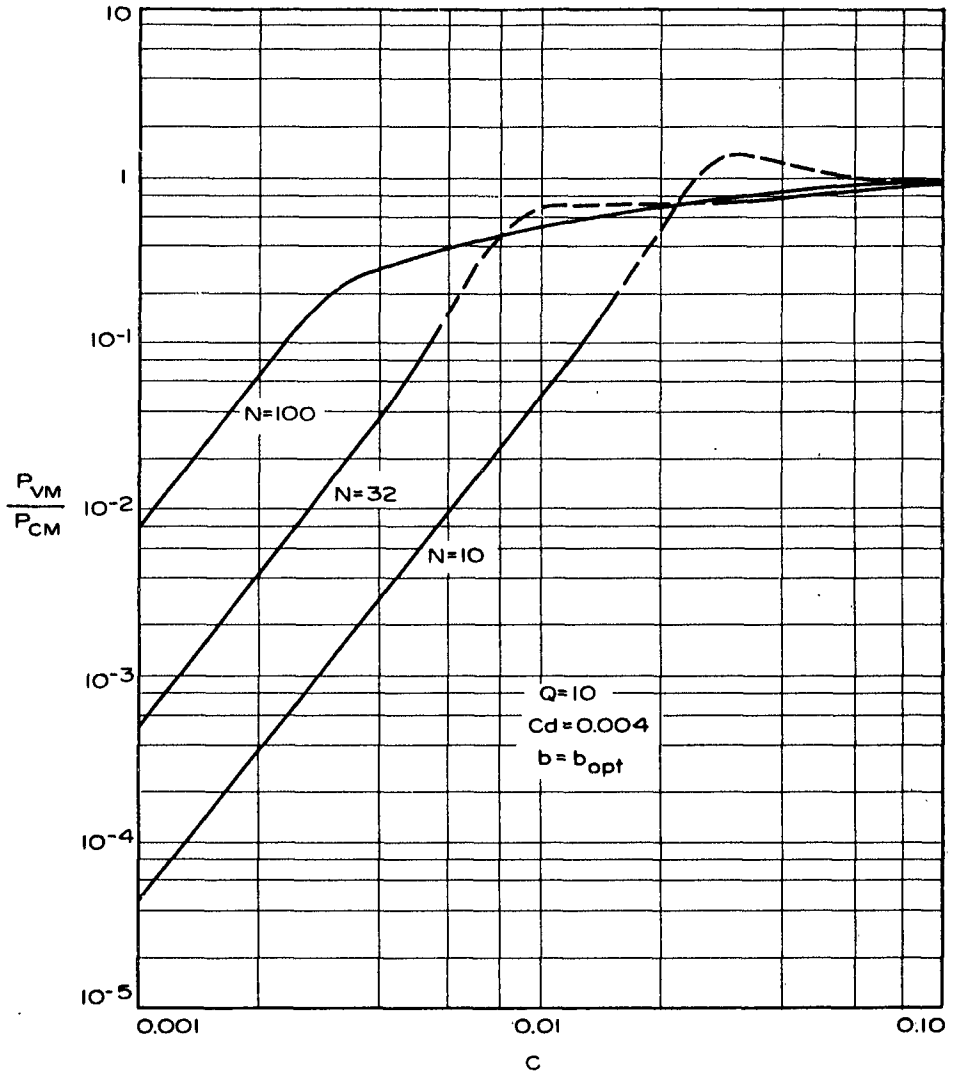

Figure 10. Comparison of Power Outputs from Current Modulation and Velocity Modulation Inputs.

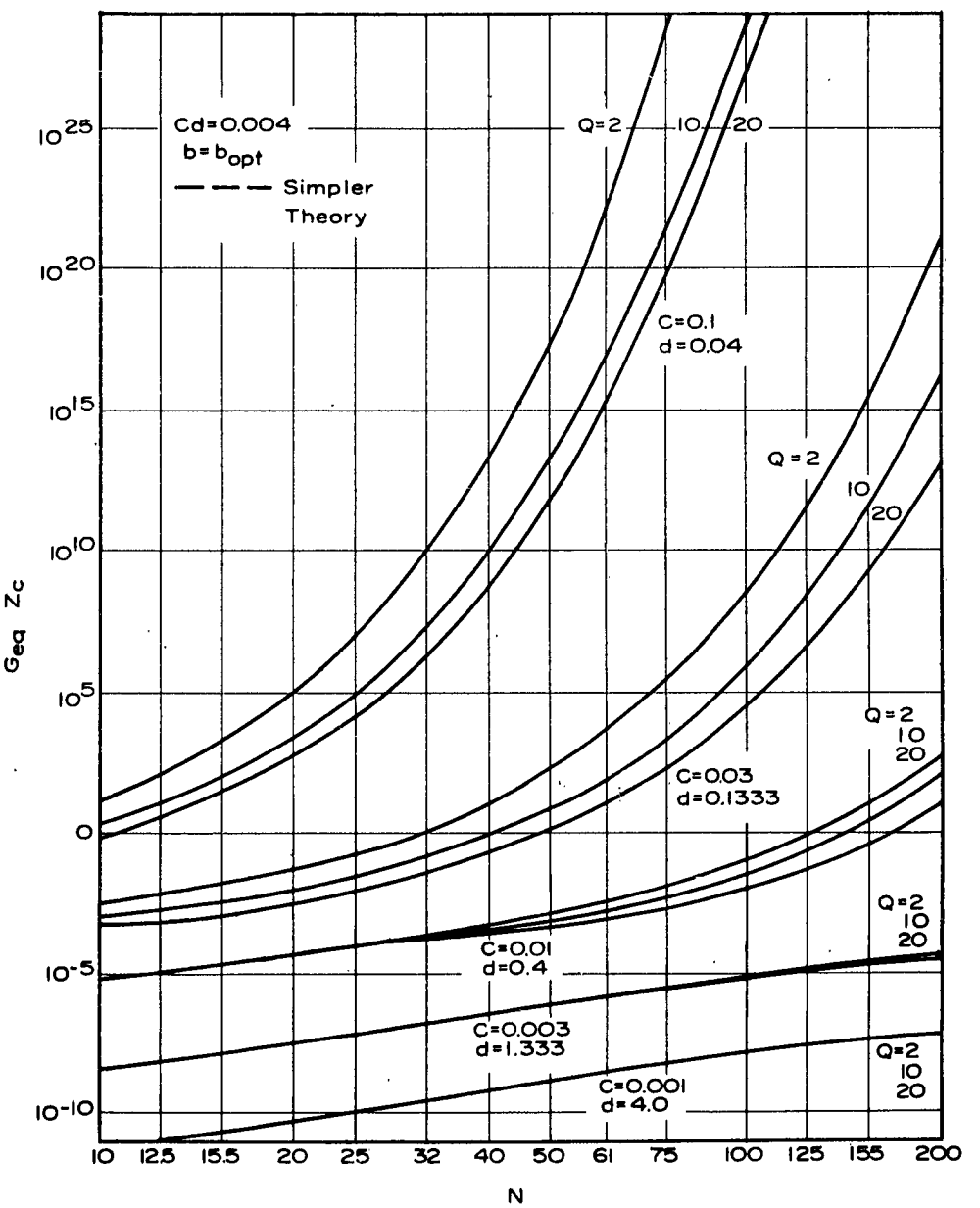

Figure 11. Dependence of Equivalent Conductance on Circuit Length. Cd = 0.004, b = optimum value for each C, N, Q.

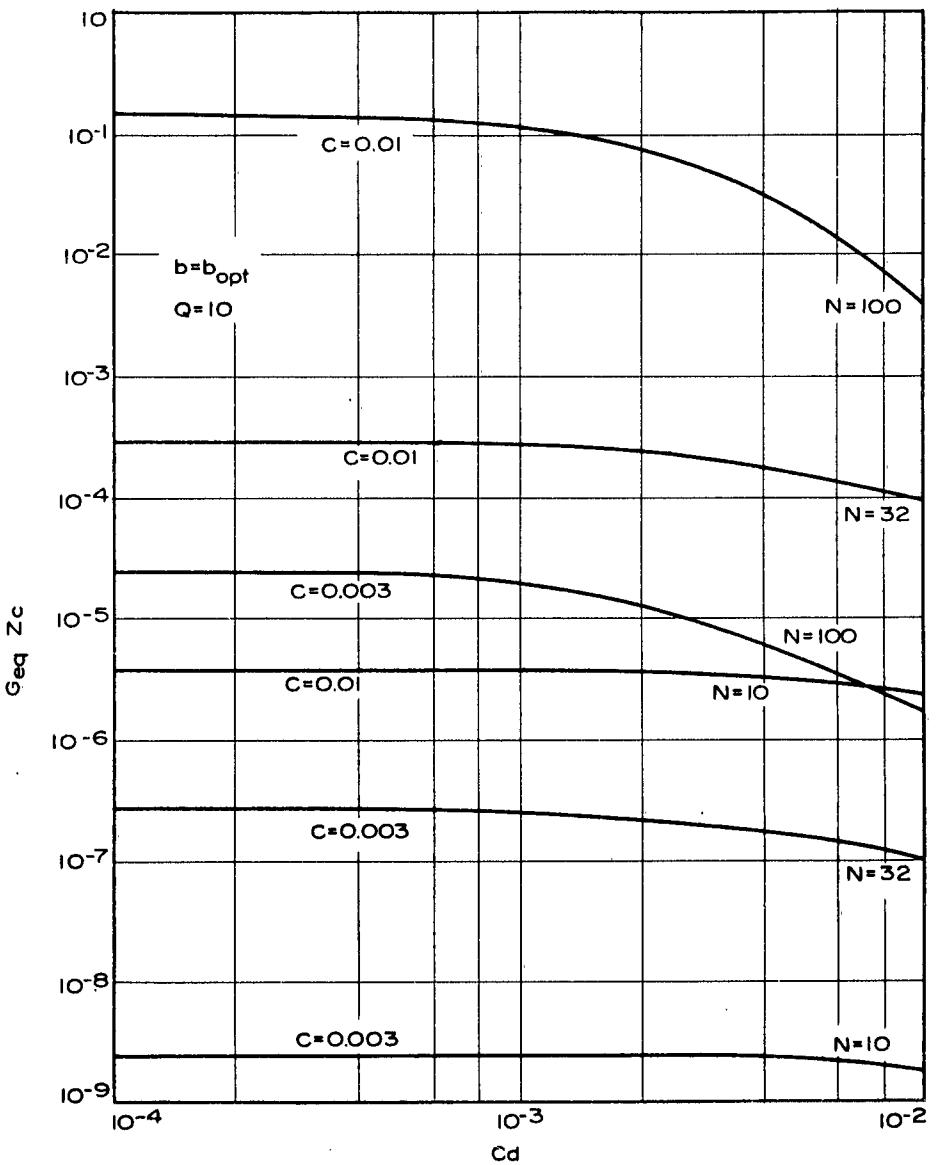

Figure 12. Effect of Circuit Loss on Equivalent Conductance Q = 10, b = optimum value for each C, N.

than that of R_{eq} (Figure 5, IER 3) seems to be that since the velocity modulated beam is slower to transfer energy to the circuit, it also loses less energy in the beginning length of the circuit.

In Figure 13 is shown a comparison of the velocity-dependence characteristics of the three types of excitation. This graph demonstrates our earlier statement about the "transfer function hierarchy". The narrowing of the curves for various circuit lengths is a good indication of the efficiencies of the three excitation schemes. It is worth repeating the reason for the differences: the circuit power input must first velocity-modulate the beam, requiring circuit length, the velocity modulation then drifts into current modulation, taking more length before the beam is in the optimum form for delivering energy to the circuit. Velocity modulation input requires only the last two steps of this process, and current modulation only the final step.

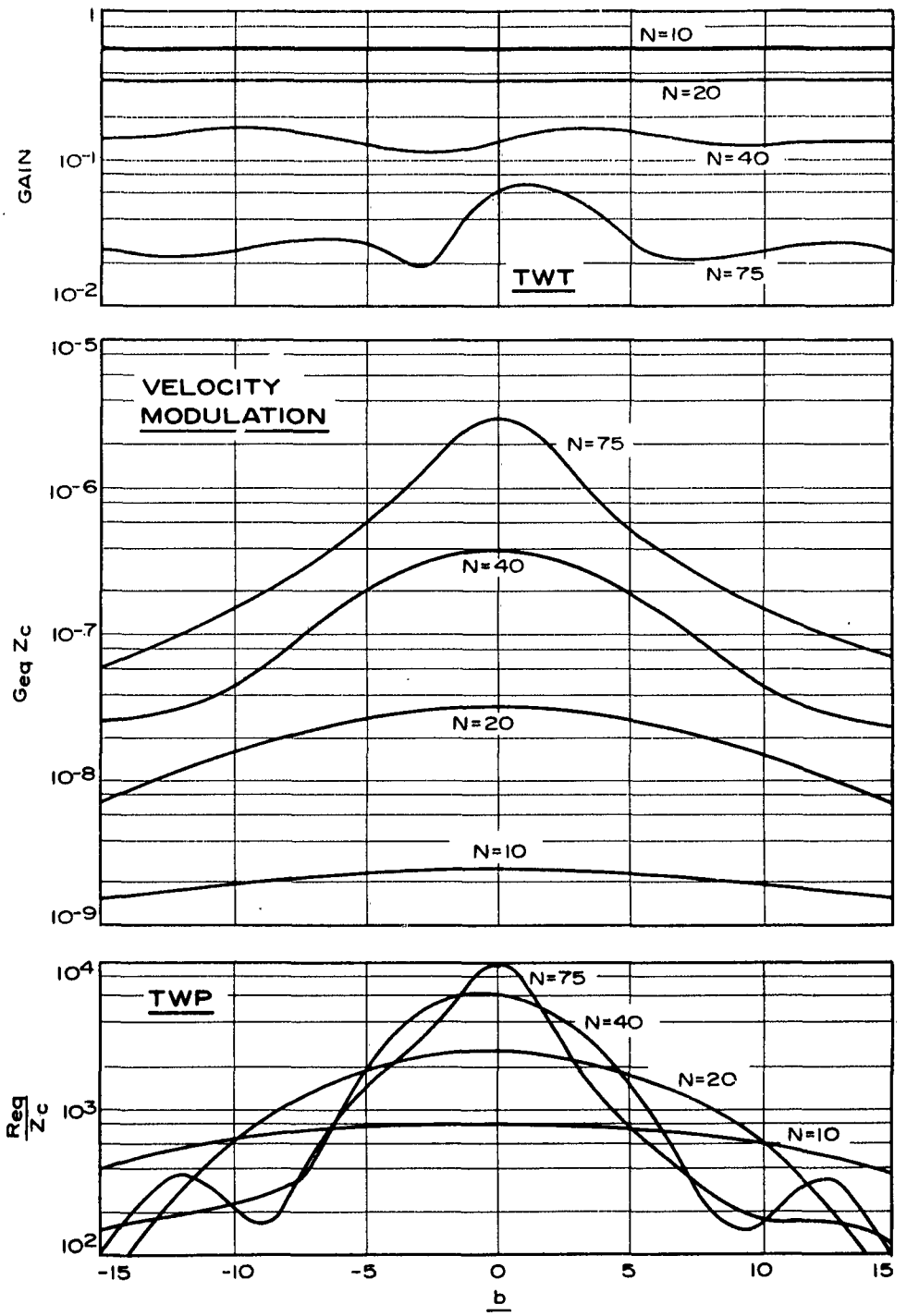

Figure 13. Comparison of Responses of the "Pure" Excitations to Changes in Beam Velocity. C = 0.003, Cd = 0.004, Q = 10.

3.5 Conclusions

Theoretical analyses have made possible a better understanding of the detailed operation of traveling-wave phototubes and have pointed out important performance characteristics to be considered in future TWP design.

An approximate analysis of the propagation of microwave signals in the photoelectron gun region has indicated that the reduction of the current modulation on the beam will be small for typical TWP operating conditions. Gun region effects should, however, be taken into account whenever the beam current approaches one-half the value for space-charge limited operation. At these higher current levels there is significant conversion of current modulation into velocity modulation and the input to the beam-helix interaction region must be treated as a combination of the two types of excitation rather than as pure current modulation.

A more accurate gun region theory based on the transmission-line analogy has been formulated but the rather involved computations have not been performed. The simpler theory seems adequate at present, although the design of guns specifically for high current operation (e.g., for optical heterodyning) may demand the more rigorous treatment.

An analysis of the effect of the high initial velocities typical of photoelectrons on TWP power output has been performed. The only case for which initial velocities need be considered is for very long tubes operating at very low voltages.

A detailed analysis of the beam-circuit interaction process has been performed.

We defined the transfer functions R_{eq} and G_{eq} which relate the circuit power output to the current modulation and velocity modulation inputs by

$$P_{out} = \frac{1}{2} |i|^2 R_{eq} + \frac{1}{2} |V_1|^2 G_{eq}$$

A high speed digital computer was used to obtain values of R_{eq} and G_{eq} that include the effects of loss, space charge and asynchronous beam velocity. These data were presented graphically for a wide range of tube parameters; they brought out several factors which are important in understanding, designing and using TWP's as a broadband light demodulators. In particular: (1) the mode-width (i.e., the range of beam voltage over which the output power is within 3 db of its maximum value) narrows substantially with increasing circuit length, and the optimum beam voltage increases with increasing average current; (2) R_{eq} is independent of average current for $CN \ll 0.3$, grows exponentially for $CN > 0.4$, and can actually decrease with increasing average current or helix length in the intermediate range of CN; (3) high circuit loss more seriously degrades the performance of longer tubes; (4) at the low average current levels often encountered in TWP operation a given beam-circuit combination operated as a TWP shows significant interaction for much shorter circuit lengths than those required of the same system used as a TWT amplifier; and (5) the clear superiority of current modulation excitation over other inputs at small CN rapidly vanishes as CN becomes large enough to permit exponential growth of circuit power.

Although this analysis is directly applicable to the TWP, it is important to note that R_{eq} and G_{eq} are completely general. That is, these results can be used in discussing any device in which traveling-wave circuits are excited by modulation on an electron beam.

SECTION IV

EXPERIMENTAL ANALYSIS OF MICROWAVE PHOTOTUBES

4.1 Objective

The purpose of this investigation is to examine experimentally the output power, bandwidth and mode-width of traveling-wave phototubes as a function of photocurrent, beam voltage and interaction length. A comparison of the experimentally determined quantities is then to be made with the values predicted by the theory.

4.2 Introduction

In this reporting period we have endeavored to perform sufficient experiments to allow for a complete description of the traveling-wave phototube in the region of normal operation. This report will describe measurements of equivalent resistance for the entire range of operating currents which the tube would be likely to encounter in operation as a detector of low level signals, or the much larger signals associated with heterodyne detection where a relatively powerful local oscillator is employed. Thus, cathode currents from 1 to 100 microamperes are examined to determine the tube's behavior well into the exponential growth region. For the purposes of these experiments we fabricated an S-band tube which, except for having an 8-inch long helix, is identical to the SYD-4302; parameters are summarized in Table I . This tube was supplied with an output coupler of the coupled helix type, mounted so that it could readily be moved along the main helix, allowing us to change the interaction length of the tube at will. This permitted us to make measurements of R_{eq}, mode-width and bandwidth as a function of interaction length as well as current and beam voltage.

It will be seen from the data presented in the following sections that there is excellent agreement between the theoretical predictions

TABLE I

EXPERIMENTAL TUBE PARAMETERS

Cathode diameter	0.070 inch
Mean helix diameter	0.104 inch
Helix TPI	62 turns per inch
Helix wire diameter	0.008 inch
Helix length (between couplers)	
"2-inch tube"	2.2 inches
"8-inch tube"	8.4 inches
Dielectric loading factor (3 Gc)	0.78 inch
Longitudinal Interaction Impedance	
f = 2 Gc	150 ohms
3 Gc	50 ohms
4 Gc	20 ohms

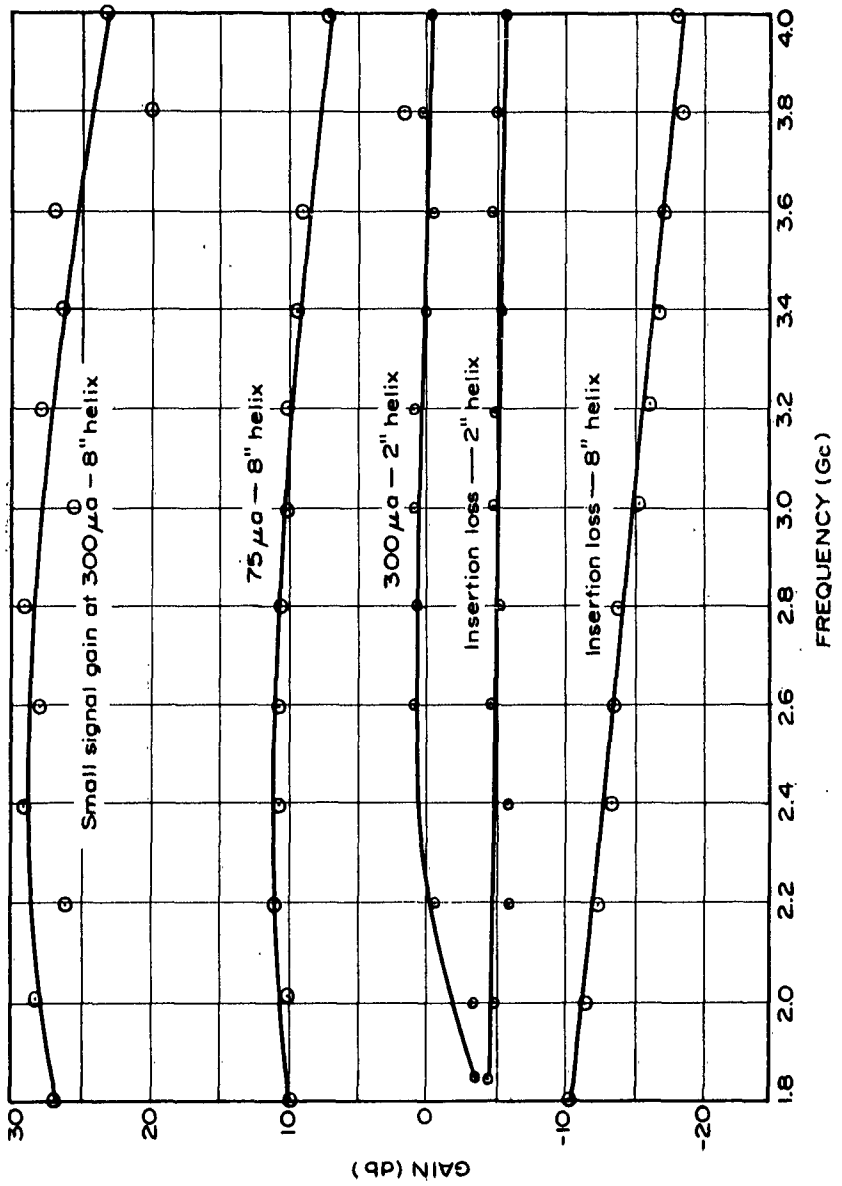

Table I (Continued)

for the tube and its actual performance. In Table II we briefly summarize the data shown in detail later.

4.3 Measurements

In previous reports we have shown that the power output from a photodetector can be given in terms of an equivalent resistance, such that the power $P = 1/2\ i^2 R_{eq}$, where i is the a-c portion of the photocurrent. Measurements of R_{eq} reported in Interim Engineering Report No. 3 gave a value of 40 to 50 thousand ohms for a two-inch interaction length and currents of a few microamperes. In this report we have extended the measurements to include two sets of parallel data covering both two inch and eight inch interaction lengths and a very wide range of cathode currents and beam voltages for frequencies in the 2-4 Gc region.

These measurements were made by taking advantage of the shot noise measurements technique, in which the shot noise from the cathode current is measured in a given bandwidth at microwave frequencies. This is done instead of providing a microwave modulator at each of the frequencies at which we wish to determine the value of R_{eq}. In this type of measurement we make use of the relation $P_{shot} = 2eI_oBR_{eq}$, where P_{shot} is the shot noise power associated with the discrete nature of the electron emission, e is the electronic charge, I_o is the average cathode current, is the bandwidth of the receiver in which the shot noise is being measured, and R_{eq} is again the equivalent resistance of the TWP under the particular set of operating conditions. It should be noted that this technique may be used for measuring R_{eq} of other light demodulators, such as photodiodes[2].

In this description, we do not speak of the discrete nature of the photons at the cathode as was done in previous descriptions of the shot noise measurement technique; in the series of experiments to be outlined here, the current in the tube was derived from a thermionic cathode rather than from a photoelectric cathode. If the cathode current is definitely temperature limited so that there is no space charge cloud in front of

TABLE II

TYPICAL S-BAND TWP PERFORMANCE

Interaction Length (inches)	Beam Current (μa)	R_{eq} (K-ohms)	Mode-width (percent)	Band-width (Gc)
8	1-10	400	3.8	2-4
8	80	4,000	5.0	2-4
2	1-10	80	15	2-4
2	80	40	15	2-4

the cathode to cause quieting then there should be the same shot noise from a beam of thermal electron as one would obtain from an identical beam made up of photoelectrons. In either case the well known expression $P = 2eI_oBR_{eq}$ should be equally valid; the experimental verification of this point will be described later.

In order to undertake such measurements, it was first necessary to determine the currents which demark the regions of temperature limited operation and space charge limited operation. Figure 14 shows a plot of cathode current as a function of filament voltage, i.e. cathode temperature. These curves are plotted for three values of accelerating voltage. The curves clearly show that the cathode of this tube is temperature limited at all beam voltages, for currents below 200 microamperes. In the experiments described here the cathode current does not exceed 100 microamperes. In all of the following experiments the beam is "strong focused" in a solenoid providing 400 gauss, and the beam transmission is always at least 90%.

4.4 Experimental Apparatus

In the experiments presented here the output from the TWP was sent to a microwave receiver having a tangential sensitivity of -100 dbm. The receiver consisted of a crystal mixer fed by a HP 614 signal generator and the tube under test. The output of this mixer went to a 30 Mc, i.f. amplifier with 80 db gain and a 9 Mc bandwidth, and thence to an HP 1 kc tuned SWR meter. In this work the TWP current was modulated at a 1 kc rate, by driving the focus electrode to -80 volts with a square wave oscillator. When absolute measurements of power from the tube were desired, a comparison was made between the tube output and that obtained from a calibrated HP 614 signal generator substituted for the tube in the mixer circuit, and similarly modulated with a 1 kc square wave. The wave shape

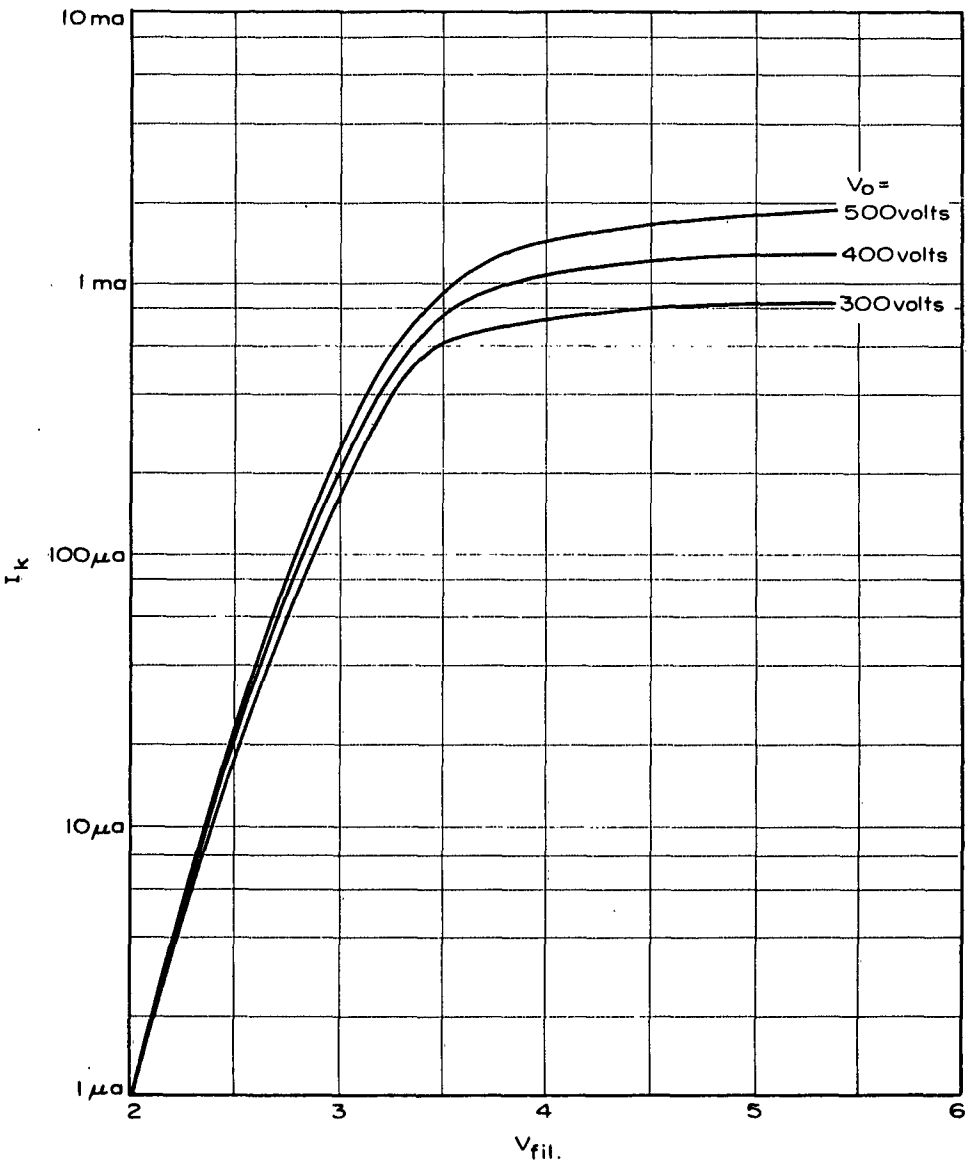

Figure 14. Thermionic Emission Characteristic of Experimental Tube.

of the tube output and the signal generator were seen to be the same when displayed of a dual beam oscilloscope. The experimental arrangement is shown in Figure 15.

4.5 R Equivalent Versus Cathode Current Measurements

R_{eq} was measured over a range of photocurrents from 1 to 100 microamperes, for both a 2-inch and an 8-inch interaction length. The measurements were all done using a single tube in which the output coupler could be moved along the helix. Thus, data reported for both the 8-inch and the 2-inch interaction length were taken from the same tube except for the position of the output coupler. This precaution was thought necessary to avoid any possible perturbation of the shot noise measurements due to differences in performance of particular tubes.

The actual measurement of R_{eq} consists of solving the shot noise equation for the equivalent resistance giving

$$R_{eq} = (2 e I_o B)^{-1} P_{SHOT}$$

Figure 16 shows the variation in R_{eq} as a function of cathode current, for currents from 1 to 100 microamperes. This variation is shown for 2, 3, and 4 Gc, and for two interaction lengths. The data show clearly the advantage to be gained from increasing length of interaction region. In the low current region of operation the change from 2 inches to 8 inches gives an improvement of approximately 6 db in output power. The longer interaction length also allows entry into the region of exponential growth for lower currents than does the shorter tube.

In Figure 17 a comparison is made between the theoretical values of R_{eq} obtained from computer calculation, together with the data taken from both thermionic and photoelectric measurements on the 8-inch interaction length. The excellent agreement among these three curves is taken as a validation of both our theory for the calculation of equivalent resistance and our measurement techniques. The data for equivalent

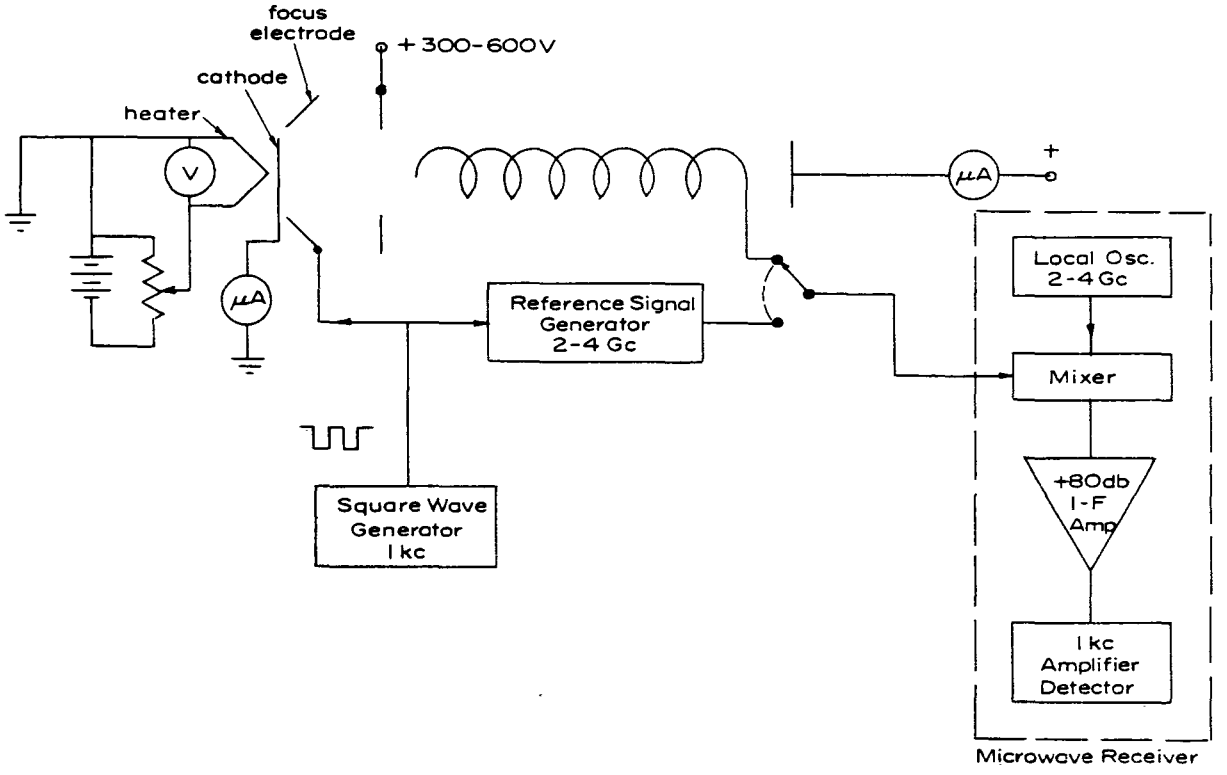

Figure 15. Experimental Apparatus for Measurement of Thermionic Tube Shot Noise.

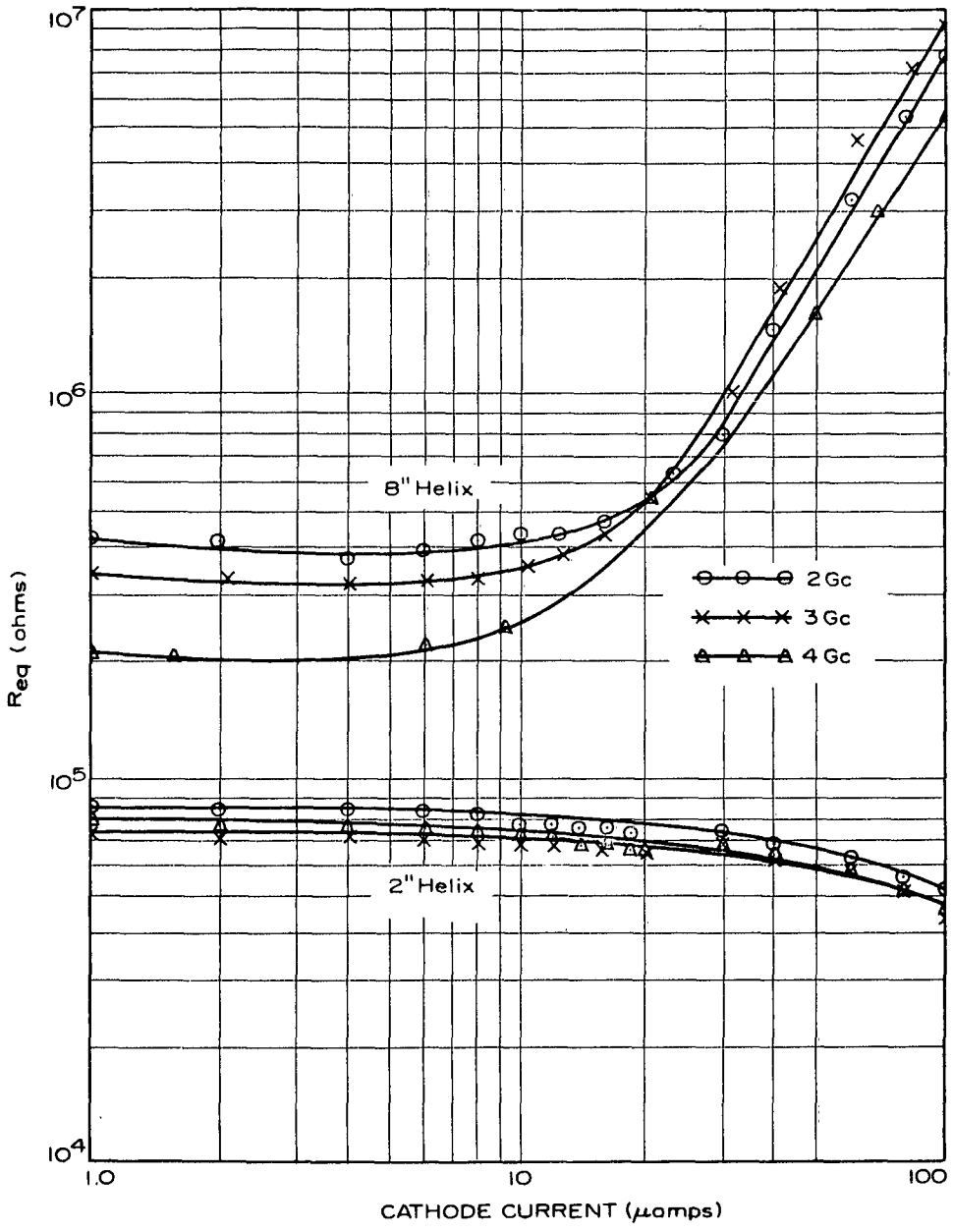

Figure 16. Measured R_{eq} Dependence Upon Beam Current

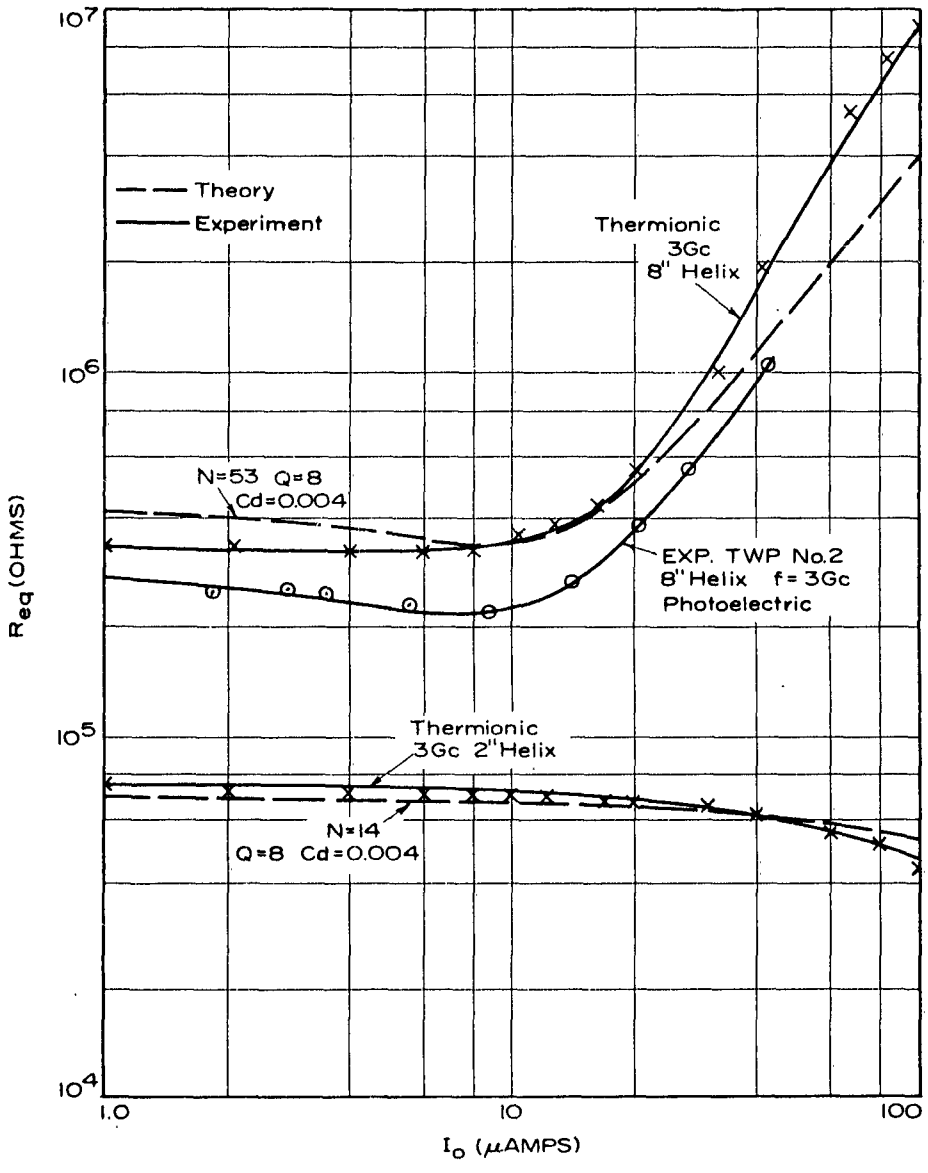

Figure 17. Comparison of Theoretical and Experimental Dependence of R_{eq} upon Beam Current.

resistance were taken with the beam voltage optimized for each of the frequencies measured. These data were taken every 100 Mc from 2 Gc to 4 Gc. The resulting plot of optimum beam voltage as a function of frequency is given in Figure 18. The variation in optimum voltage is seen not to be a strong function of the total cathode current; i.e., it varies only 5 volts over the range of currents measured. Note that the characteristic variation of synchronous voltage with frequency is observed here.

4.6 Mode-Width Measurements

The mode-width of the microwave phototube is defined as the total variation in beam voltage which produces a 3 db drop from the peak output power. Thus, the mode-width is a measure of a given tube's sensitivity to variations from the synchronism condition. Since in actual operation a tube can be operated at only a single voltage, the mode-width will strongly affect the bandwidth of the tube.

For both interaction lengths the mode-width is seen to increase with increasing cathode current. The mode-width data have been plotted separately for the two interaction lengths. The mode-width data for the 8-inch length are shown in Figure 19 and the data for the 2-inch length are plotted in Figure 20. Both of these plots show the theoretical data plotted along with the experimental curves, and the agreement is quite good in both cases. It can be seen from the curves that the shorter tube has over twice the mode-width of the longer tube. Thus, if mode-width were the only thing limiting frequency response, the shorter tube would be expected to have much greater bandwidth. The detailed measurements of mode-width for the 2-inch length will be seen to agree with the photoelectric data for mode-width reported in the third Interim Engineering Report.

4.7 Bandwidth Measurements

The bandwidth of a microwave phototube is defined as the frequency

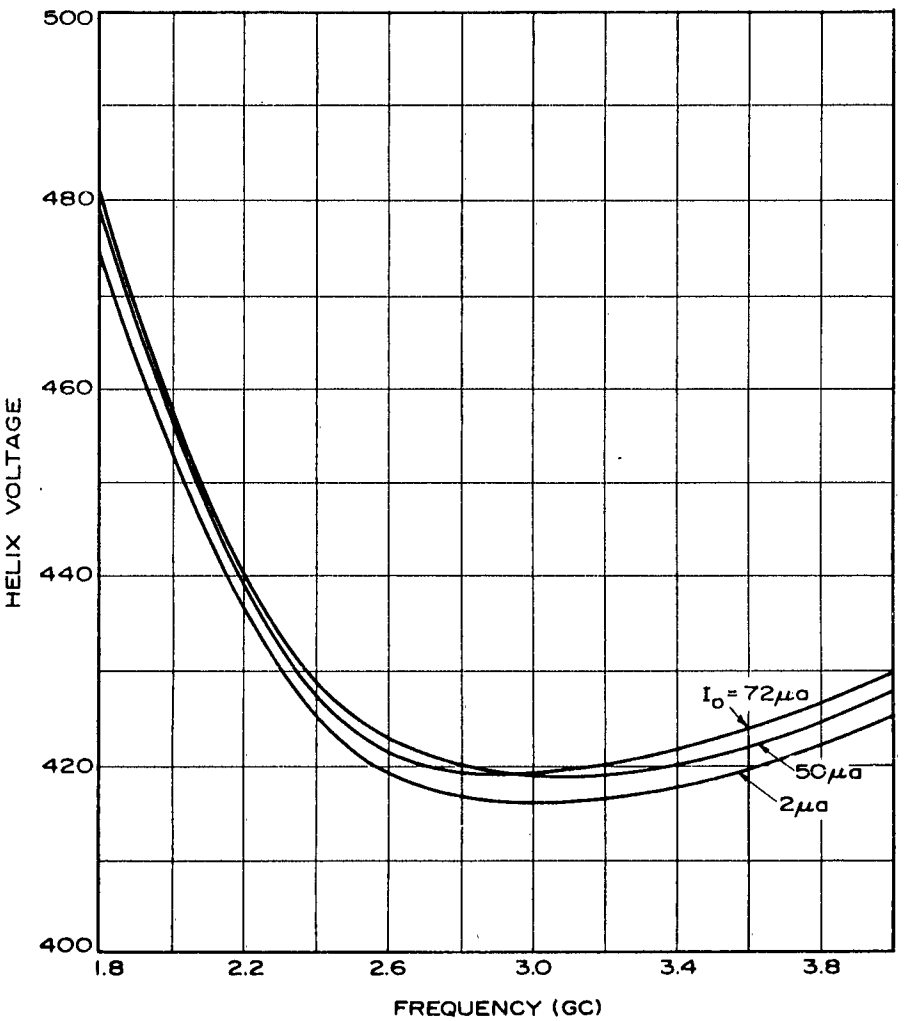

Figure 18. Optimum Beam Voltage Versus Frequency.

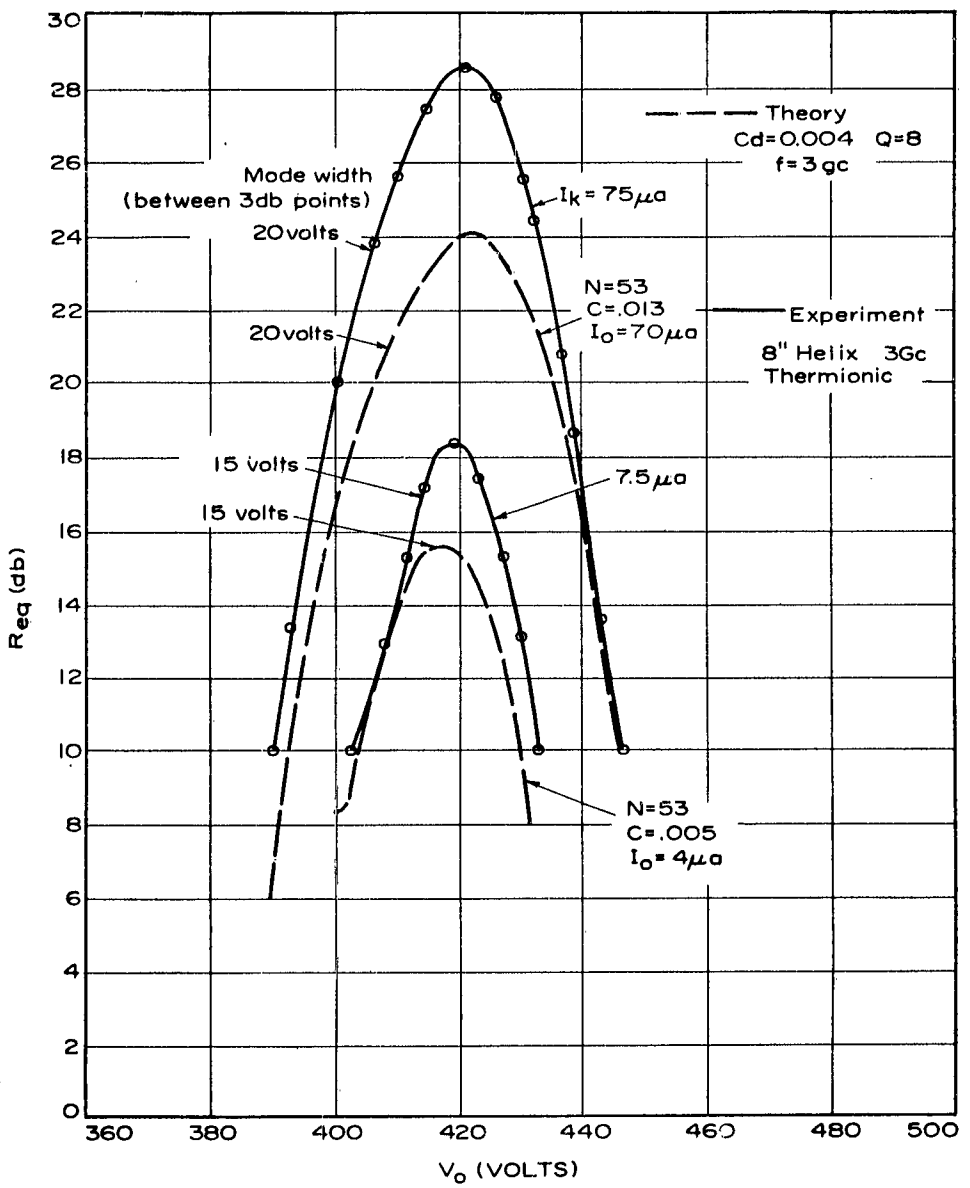

Figure 19. Mode-width of 8-inch Thermionic Tube.

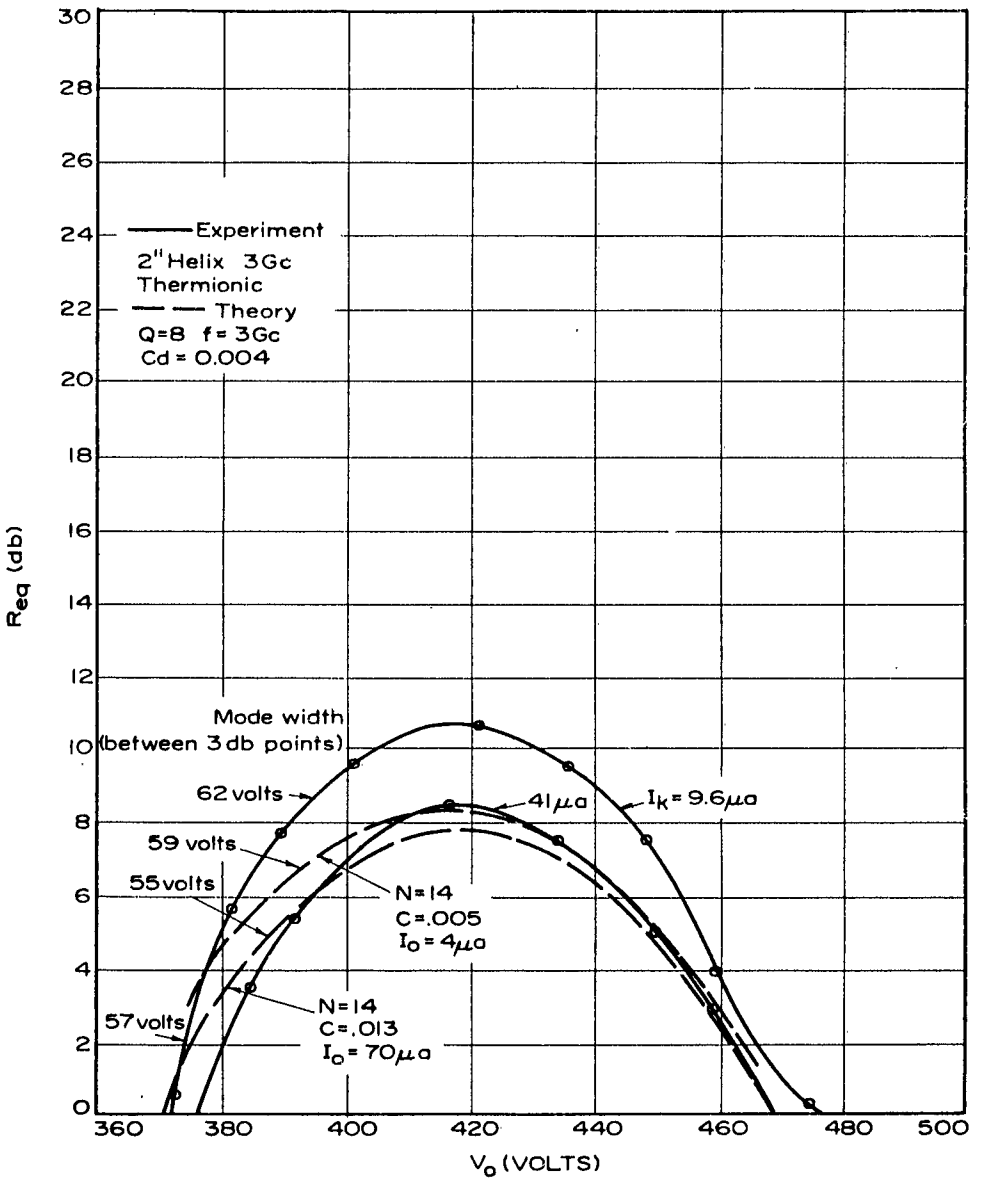

Figure 20. Mode-width of 2-inch Thermionic Tube.

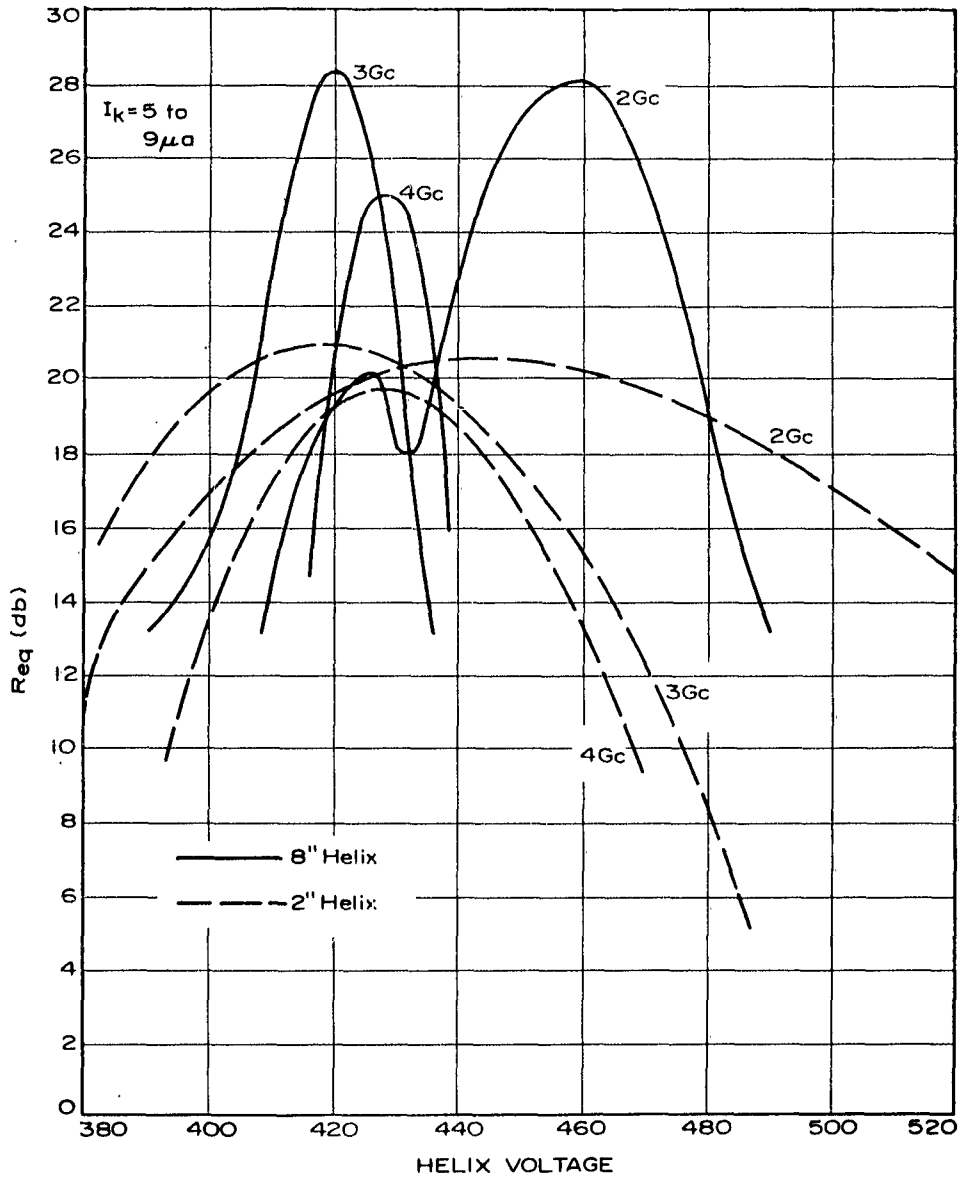

Figure 20A. Mode-width of 8-inch Tube Versus 2-inch Tube at Three Frequencies.

range over which the tube operates without suffering more than 3 db total variation in power output for a given value of the operating parameters. In such a measurement there are many possible choices for the beam voltage. We chose the voltage which is optimum for the high end of the frequency band and the voltage which is optimum for the center of the band. The data for both choices are shown in Figure 21. In all cases it is seen that the response of the device begins to fall sharply above 4 Gc. This fall is due almost entirely to a degradation of the microwave match above that frequency. In the curves where the voltage is chosen favoring the high end on the band, a dip in the center of the band is seen, with a rise at the lower frequencies. This is the result of the fact that the same voltage is optimum at the high and low ends of the band, with a different lower value of voltage optimum in the center of the band. In the case where the voltage is set at the value favoring the center of the band, a curve free of dips is obtained but the price paid is considerably reduced bandwidth. Because of the much increased mode-width of the 2-inch tube over the 8-inch length, we find that the bandwidth of the 2-inch tube is relatively insensitive to the beam voltage chosen. A median value for the band of this tube can be taken as 2 to 4.0 Gc. Of course these frequency limits are by no means cutoff points. The tube still has substantial values for R_{eq} well below 2.0 Gc and somewhat above 4.0 Gc.

4.8 Conclusions

In the experimental section of this report we have presented the results of a series of investigations into the behavior of microwave phototubes, and these results have been compared with the values obtained from our theoretical calculations. For the pertinent measurements, i.e. R_{eq} and mode-width, we have plotted the experimental and the theoretical data together. In all these measurements the data are seen to be in good agreement with the theoretical predictions. This agreement will allow us in the future to rely upon our theoretical curves and our computer

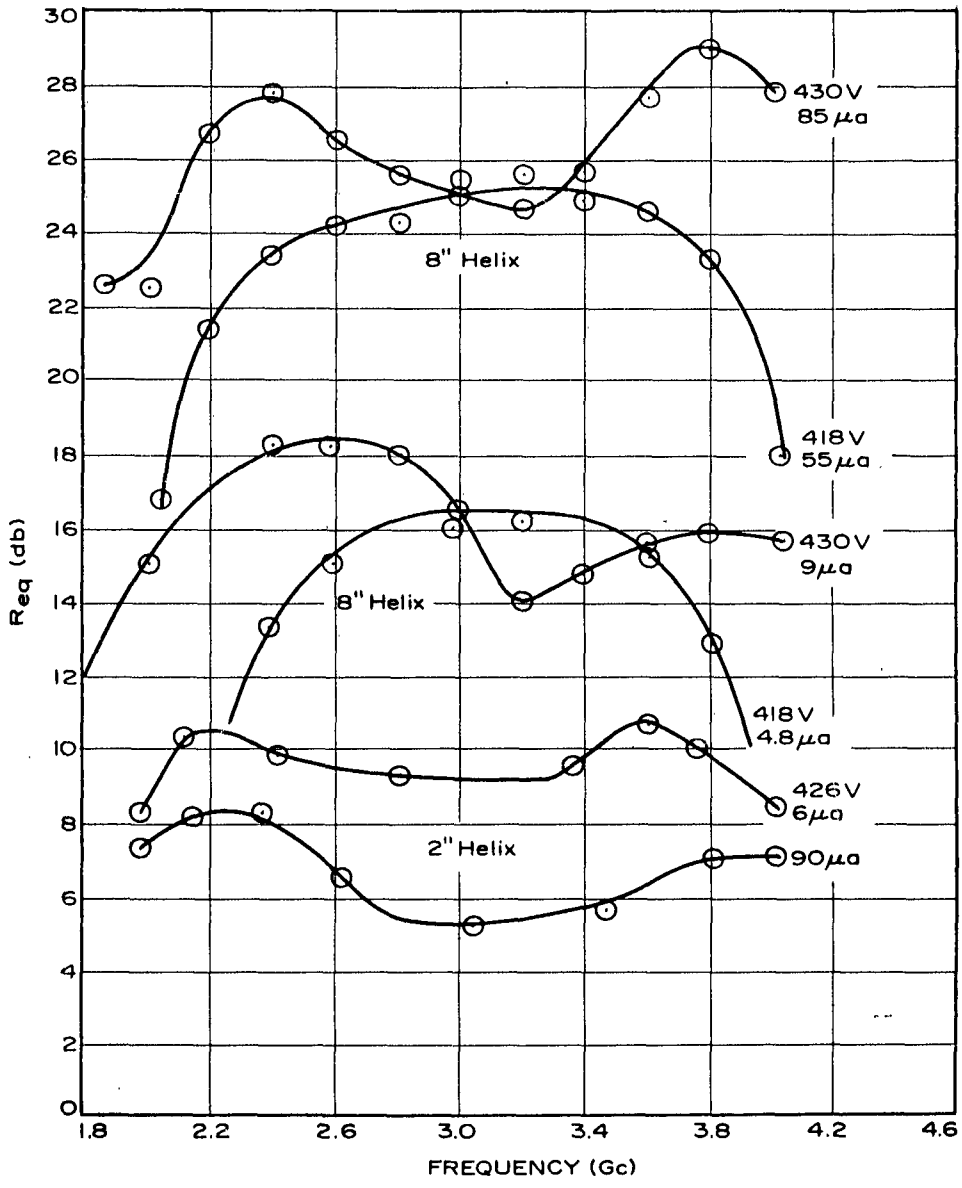

Figure 21. Thermionic Tube Bandwidth.

program for the design of subsequent microwave phototubes.

A further outcome of the experimental program is the development of the thermionic technique for measuring the response of the TWP. In our first measurements we made use of a microwave light modulator to examine the behavior of the tube as an optical demodulator. The shot noise associated with the incoming light was also measured. Values for R_{eq} obtained from these two measurements were compared and found to be in good agreement. The shot noise technique was then adopted as a method for examining TWP's. Now, since the technique using the thermally generated shot noise has shown agreement with both the previous photoelectric measurements as well as agreement with the theoretical predictions, we feel that this method should be considered as well established for use in any further investigations into the behavior of these tubes.

SECTION V

SUMMARY OF RESEARCH CONTRIBUTIONS ON AM DEMODULATORS

The major achievments of the past year's applied research on AM demodulators are briefly summarized below:

(1) At the outset of the program a background literature investigation and a theoretical investigation of various light modulation detectors were carried out. These investigations led to the conclusion that the helix-type traveling-wave phototube (TWP) was the most promising method of light modulation detection consistent with the objectives of the program.

(2) A simplified theoretical analysis (i.e., neglecting loss and space charge, and assuming synchronous velocity) was carried out for the TWP, and the results indicated that the TWP differs from the conventional TWT in more respects than were at first obvious. In this analysis we were the first to describe the behavior of a TWP in terms of R_{eq}, the "equivalent resistance" or "effective resistance" and G_{eq}, the "equivalent conductance" or "effective conductance". Further, we developed a complete noise theory for the TWP and calculated the effects of thermal noise, shot noise and velocity-fluctuation noise.

(3) C-w microwave modulation-demodulation experiments using TWP's (preceded only by the preliminary experiments of Harris, McMurtry and Siegman at Stanford) were performed, and the results were quite close to the predictions of our simplified theory.

(4) A considerably more accurate theory was developed to include the effects of loss, space charge, asynchronous velocity and

finite C. Results obtained with the use of a high speed digital computer showed several important effects that had not been apparent from the simplified theory.

(5) Comprehensive measurements of R_{eq}, mode-width and bandwidth were performed using both the modulation-demodulation technique and the shot-noise technique for measuring R_{eq}. (This latter technique was suggested independently and used by L. K. Anderson at Bell Telephone Labs in his work on solid-state photodiodes.) Measurements were performed over a wide range of frequency, voltage, helix length and average current.

(6) In addition to verifying the validity of the shot-noise technique for measuring R_{eq} in tubes with photoelectric cathode, we proposed and verified that R_{eq} for a particular TWP structure can be accurately measured using temperature-limited thermionic emission.

(7) Detailed comparison of the comprehensive measurements with the more accurate theory showed extraordinarily good agreement, which indicates that the theory can be relied upon for future TWP designs.

(8) The effect of the large spread in initial electron velocities for phototelectric cathodes was investigated theoretically, and it was found that there was essentially no degradation in output power except for extremely long tubes operated at very low helix voltage.

(9) Two different theoretical techniques were used to examine the conversion of current modulation to velocity modulation in the gun region of a TWP. The results indicated that there is less than 3 db degradation in power output for currents up to about one-half of the space-charge limited current.

(10) Theoretical investigations of other light modulation detectors were carried out all during the program, and new devices were compared to the TWP. In addition, some direct experimental comparisons were performed using TWP's, solid-state photodiodes, and bulk mixers using CdSe. The conclusion of these investigations was that the TWP still appears to be the most promising light modulation detector consistent with the objectives of this program.

SECTION VI
CONCLUSIONS

This report and the three previous Interim Engineering Reports provide sufficient information for the detailed understanding, design and use of traveling-wave phototubes (TWP's). It has been shown that they exhibit all of the characteristics sought at the outset of this program; i.e:

(1) Capability of detecting light signals modulated at microwave frequency rates;
(2) Capability of detecting with large modulation bandwidths (greater than 1 Gc);
(3) Suitability for optical heterodyne detection;
(4) Capability of amplification in the light modulation detector; and
(5) Low noise detection.

Detailed conclusions concerning the work this quarter are presented in Sections 3.5 and 4.8.

In addition, a Summary of Research Contributions on AM Demodulators has been provided in Section V of this report.

SECTION VII

RECOMMENDATIONS

It is recommended that the program outlined in Section VIII be carried out.

SECTION VIII
PLANS FOR NEXT PERIOD

The proposed program for the next period is to perform a background literature investigation and a theoretical investigation of techniques for demodulating microwave frequency modulated (FM) light. The investigation is to include, but not be limited to, transverse-wave microwave phototubes and birefringent discriminators.

SECTION IX

REFERENCES

1. L. D. Smullin, "Propagation of Disturbances in One—Dimensional Accelerated Electron Streams", Journal of Applied Physics, Vol. 22, pp 1496-1498, December 1951.

2. L. K. Anderson, "Measurement of the Microwave Modulation Frequency Response of Junction Photodiodes", Proceedings of the IEEE, Vol. 51, No. 5, pp 846-847, May 1963.